

# Design and Numerical Optimization of RF pulses for NMR quantum computing

**Saksham Mahajan**

*A dissertation submitted for the partial fulfilment of BS-MS dual degree  
in Science*



Indian Institute of Science Education and Research, Mohali

May 23, 2021

## Certificate of Examination

This is to certify that the dissertation titled "Design and Numerical Optimization of RF pulses for NMR quantum computing" submitted by Saksham Mahajan (Reg. No. MS16068) for the partial fulfilment of BS-MS dual degree program of the Institute, has been examined by the thesis committee duly appointed by the Institute. The committee finds the work done by the candidate satisfactory and recommends that the report be accepted.



Prof. Arvind



Dr. Satyajit Jena



Prof. Kavita Dorai  
(Supervisor)

Dated: May 23, 2021

## Declaration


The work presented in this dissertation has been carried out by me under the guidance of Prof. Kavita Dorai at the Indian Institute of Science Education and Research Mohali. This work has not been submitted in part or in full for a degree, a diploma, or a fellowship to any other university or institute. Whenever contributions of others are involved, every effort is made to indicate this clearly, with due acknowledgement of collaborative research and discussions. This thesis is a bonafide record of original work done by me and all sources listed within have been detailed in the bibliography.



Saksham Mahajan  
(Candidate)

Dated: May 23, 2021

In my capacity as the supervisor of the candidate's project work, I certify that the above statements by the candidate are true to the best of my knowledge.



Prof. Kavita Dorai  
(Supervisor)

## **Abstract**

Quantum computing is at the leading edge of scientific and technological research of the 21st century. In today's world, scientists have found a good number of approaches towards quantum information processing like superconducting qubits, trapped ion systems, spin based magnetic resonance etc. Out of all these Nuclear Magnetic Resonance has evolved as an excellent test bed for testing of quantum protocols.

In this thesis we explored the idea of NMR Quantum Computing. Our study has focused on two different themes. Initially, we explored the concept of pseudo pure state which is widely used while performing NMR Quantum Computation. This thesis provides an entirely new sequence that has been developed for creating a pseudo pure state in a hetero nuclear four qubit system.

The latter part of the thesis focuses on the existing problem of low fidelity while performing quantum computation with large number of qubits. Therefore, we explored and implemented the idea of using Optimal Control Theory for pulses designing. We have focused on using Gradient Ascent Pulse Engineering (GRAPE) for the numerical optimization of pulses. All the experiments have been performed on two qubit homo nuclear system as a test sample.

We have also explored the concept of Quantum State Tomography. This concept has been introduced to find the experimental fidelity of the states obtained.

## Acknowledgements

If I have seen further it is by standing on the shoulders of Giants

- Sir Isaac Newton

I would like to extend my deepest gratitude to my Master's thesis supervisor, Prof. Kavita Dorai, without whose constant support this thesis would not have been possible. Her continuous guidance in discussions, exchanging ideas, and moral support whenever required helped me complete this thesis on time and develop some remarkable results.

I would like to thank my Master's thesis committee members, Prof. Arvind and Dr. Satyajit Jena, to agree to be a part of my committee and provide me with important feedback.

I would also like to thank Vaishali Gulati (PH.D. fellow at IISER Mohali), for her help in performing the experiments and for mentoring me throughout my master's journey. This thesis would not have been possible without the various informative discussions that we had over time.

I would also like to thank Dileep Singh, Akshay Gaikwad and Krishna Shende for productive discussions that kept me on track during the whole journey. I would also extend my thanks to Sumit Mishra, Akanksha Gautam, Jyotsana Ohja, Balbir Singh, Himanshu Joshi, Omkar Bihani and Divyanshi for being supportive lab members.

Finally, I would like to thank my friends (in alphabetical order) Anubhav Kumar Shrivastva, Abhishek Mickz, Abhishek Purohit, Anmol Arya, Bhavesh Rajgopal, Bhumiya Gautam, Chahat Badhan, Hiral Gandhi, Kirti Giroh, Nandini Garg, R. Bharathkumar, Samyak Prasad, Sparsh Tyagi, Sonell Malik, Utkarsh Pathak, Vishal Varma, my parents (Mrs.) Mandeep Kumari and Mr. Rajesh Mahajan, and my family members for their constant support and help, which kept me motivated and inspired me to finish this thesis on time.

# List of Figures

2.1	Spin orientation and energy level splitting caused by Zeeman effect in spin 1/2 system . . . . .	3
2.2	More spins precess around the direction parallel to field than against it, giving rise to net macroscopic magnetization which points in the direction of the field. [8] . . . . .	4
2.3	The rotating frame axis with reference to the lab frame ( $\omega_0 = \omega_{ref}$ ). . . . .	7
2.4	The pulse sequence used to measure the longitudinal relaxation. . . . .	10
2.5	The pulse sequence used to measure the $T_2$ time scale. . . . .	11
4.1	Decision flow chart for choice of numerical optimization method. [4] . . .	21
4.2	Schematic representation of a control amplitude $u_k(t)$ , consisting of N steps of equal duration $\Delta t$ . The Vertical arrows represent respective gradients indicating how each amplitude should be modified in the next iteration to improve the performance function under consideration.[5] . . . . .	23
4.3	Schematic representation of NMR and with effective field value parameters	25
4.4	The above tree diagram represents how each loop proceeds to incorporate the RF miscalibration error. . . . .	26
5.1	Molecular structure of cytosine with the two qubits labeled as $H^1$ and $H^2$ and the system parameters with chemical shifts $\nu_i$ , coupling $J_{12}$ (in Hz) and relaxation times $T_1$ and $T_2$ (in seconds).[14] . . . . .	28
5.2	NMR spectrum obtained after a $\pi/2$ rotation pulse on the thermal equilibrium state. . . . .	28
5.3	This file contains the information about the amplitude and direction of the transverse magnetic field to be applied at every time step. . . . .	29
5.4	Selective $\pi/2$ rotation of qubit 1. . . . .	30
5.5	Selective $\pi/2$ rotation of qubit 2. . . . .	31
5.6	Quantum circuit for creating two qubit pseudo pure state. . . . .	32
5.7	PPS spectrum after II tomography pulse. . . . .	33
5.8	PPS spectrum after IX tomography pulse. . . . .	34
5.9	PPS spectrum after IY tomography pulse. . . . .	34

5.10 PPS spectrum after XX tomography pulse. . . . .	35
5.11 X-gate spectrum after II tomography pulse. . . . .	39
5.12 X-gate spectrum after IX tomography pulse. . . . .	39
5.13 X-gate spectrum after IY tomography pulse. . . . .	40
5.14 X-gate spectrum after XX tomography pulse. . . . .	40
A.1 Spectrum and deviation density matrix obtained after hard $\pi/2$ pulses. . .	43
B.1 Frequency response of ideal low pass filter . . . . .	45

# Contents

<b>List of Figures</b>	<b>i</b>
<b>1 Introduction</b>	<b>1</b>
1.1 Motivation and Problem Statement . . . . .	1
<b>2 Basics of NMR</b>	<b>2</b>
2.1 General Principle . . . . .	2
2.2 Interaction With Static Magnetic Fields . . . . .	3
2.3 Interaction with the Radio Frequency Field . . . . .	5
2.3.1 Vector Model . . . . .	5
2.3.2 Relation between lab and rotating frame . . . . .	7
2.4 Ensemble of spins . . . . .	7
2.4.1 Concept of Density matrix . . . . .	7
2.5 The Theory of Relaxation . . . . .	9
2.5.1 Longitudinal Relaxation . . . . .	10
2.5.2 Transverse Relaxation . . . . .	11
2.6 Important Nuclear Spin Interactions . . . . .	12
2.6.1 Chemical Shift . . . . .	12
2.6.2 J-coupling . . . . .	12
2.6.3 Dipolar Coupling . . . . .	13
2.6.4 Quadrupolar Coupling . . . . .	13
<b>3 Pseudo Pure State</b>	<b>14</b>
3.1 Theory . . . . .	14
3.2 Spatial Averaging . . . . .	15
3.3 Sequence generated for 4 qubit system(Result) . . . . .	16
3.4 Product Operator Analysis . . . . .	18
<b>4 Optimal Control Using GRAPE</b>	<b>19</b>
4.1 Motivation . . . . .	19
4.2 Optimal control in NMR . . . . .	20
4.3 Theory of GRAPE . . . . .	20



4.3.1	Transfer between Hermitian operators . . . . .	20
4.3.2	Synthesis of Unitary Transformations . . . . .	23
4.4	Basic Algorithm . . . . .	24
4.5	Features of the code written . . . . .	24
4.5.1	Robustness against offset error . . . . .	24
4.5.2	Robustness against RF Miscalibration . . . . .	25
4.5.3	Reduction of RF Power . . . . .	25
4.5.4	Smooth Initial and Final controls . . . . .	25
4.6	Bandwidth Control . . . . .	26
<b>5</b>	<b>Results Obtained</b>	<b>28</b>
5.1	Two Qubit System Description . . . . .	28
5.2	Output File . . . . .	29
5.3	Single Qubit Rotations . . . . .	29
5.4	Two Qubit Pseudo pure state . . . . .	32
5.5	Quantum State Tomography . . . . .	35
5.6	X-gate . . . . .	38
<b>6</b>	<b>Summary and Conclusion</b>	<b>41</b>
6.1	Tasks Completed . . . . .	41
6.2	Future Scope . . . . .	41
<b>A</b>	<b>Spectrum Information</b>	<b>43</b>
<b>B</b>	<b>Interpolation and Filtering</b>	<b>44</b>
B.1	Convolution Theorem . . . . .	44
B.2	Ideal Low pass filter . . . . .	44
	<b>Bibliography</b>	<b>46</b>

# Chapter 1

## Introduction

### 1.1 Motivation and Problem Statement

Today, "Quantum Computing" is one of the most rising fields. The potential that quantum computers offer is solving certain problems inaccessible to classical computers because their scale or complexity is enormous. The focus has now shifted from building a quantum computer to building a scalable quantum computer.

All this requires years of research. The basic requirements to carry out quantum computation are Characterization of the quantum state, initialization, gate implementation and measurements. All the requirements are satisfied by several approaches that scientists have developed over the years. Nuclear Magnetic Resonance is one such technique that has emerged as the testbed for quantum protocols because of the high level of control that it offers. NMR, as the name suggests, deals with nuclear spins. Since no physical system can be completely isolated from its surroundings, this imposes a fundamental restriction on the potential of the NMR systems in the form of Decoherence. Also, since different nuclear samples involve different nuclei with different chemical environments, so they all can't be handled efficiently by using similar RF pulses. The control fields need to be tailored according to the system at hand to exercise the best possible control over the system. This is where numerical optimization of the NMR pulses comes into play.

Deriving the motivation from the necessity of numerical optimization, in this study, we have tried to analyze the numerical optimization methods that exist. This thesis demonstrates how numerical optimization can be used to perform selective excitations and its use to achieve high fidelity results.

# Chapter 2

## Basics of NMR

### 2.1 General Principle

The phenomenon of nuclear magnetic resonance can be observed for nuclei having non-zero angular momentum. Nuclear angular momentum is generally called nuclear spin. In the formalism of quantum mechanics, it is represented by  $\hbar\mathbf{I}$ , where  $\mathbf{I}$  is the dimensionless operator representing the total angular momentum of the nucleus. The formalism for the nuclear spin remains the same as it is for the total angular momentum. In most usual NMR experiments, the magnitude of energy involved is much lower than the spacing between the ground and excited nuclear levels. Therefore, we can be sure that the nucleus remains in the ground state during the whole experiment and all the states of interest are contained in the vector subspace spanned by vectors  $|I, m\rangle$  where  $\mathbf{I}$  is fixed.

The total angular momentum of the nucleus is due to the contribution of all the orbital and intrinsic angular momenta of the protons and neutrons constituting the nucleus. The nucleus's net angular momentum is defined by the pairing of these nucleons inside the energy levels of the nucleus (taking into consideration the Standard Model of Nuclear Physics). All the nuclei having a non-zero nuclear spin possess a magnetic dipole moment ( $\mu$ ). Like angular momentum, the nuclear magnetic dipole moment is also the result of the composition of all the nucleons' magnetic dipole moment. In fact these two can be directly related with the help of a result from the theory of angular momentum, known as the Wigner-Eckart theorem.[9]

$$\mu = \gamma_n \hbar \mathbf{I} \quad (2.1)$$

where  $\gamma_n$  is called the gyromagnetic ratio of the nucleus and is characteristic of nuclear species. The point to note here is that the magnetic dipole moment is not strictly parallel to the vector  $\mathbf{I}$  and is on an average given by its projection on the axis defined by  $\mathbf{I}$ . This is an effective solution as long as the nucleus stays in its ground state, and the total angular momentum of the nucleus is kept constant.

## 2.2 Interaction With Static Magnetic Fields

Nuclei with non zero angular momentum interact with the electromagnetic field around them through nuclear dipole moments and in case nuclear spin  $> \frac{1}{2}$ , the nuclear quadrupole moments and other effects start to play a dominating role. To keep things a bit simple here, we will be working with spin 1/2 qubits which allows a fair assumption that the charge distribution is symmetric and the magnetic dipole moment will play the dominating role. An important interaction necessary to understand is the Zeeman interaction between the magnetic dipole moment and the magnetic fields existing at the nuclear site. In simple words, Zeeman interaction gives rise to a manifold of energy levels for the nucleus depending on its orientation with respect to the axis which is defined by the magnetic field.[8]

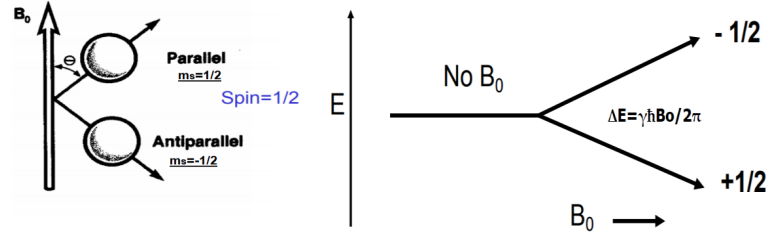


**Figure 2.1:** Spin orientation and energy level splitting caused by Zeeman effect in spin 1/2 system

Classically, the interaction between magnetic dipole moment  $\mu$  and the static field  $B_0$  can be described by the concept of orientation-dependent potential energy  $-\mu \cdot B_0$  and the torque associated with it  $\mu \times B_0$ . If the dipole moment is parallel and proportional to the body's angular momentum (which is in the case of NMR), the torque causes precession of the body about the axis of  $B_0$ . The resultant motion is called the Larmor precession and the frequency of this precession is known as the Larmor frequency.

$$\omega_L = \gamma_n B_0 \quad (2.2)$$

This is exactly what occurs for the atomic nuclei with non zero spin in the presence of the external static magnetic field. Quantum mechanically this splitting in the energy can be explained with the help of the Zeeman Hamiltonian.

$$H_Z = -\mu \cdot B_0 = -\mu_z B_0 = -\gamma \hbar B_0 I_z = -\hbar \omega_L I_z \quad (2.3)$$

This precession can also be realized with the help of quantum mechanics by calculating the expectation values of the Cartesian components of the nuclear spin operator. What we see is that  $\langle I_x \rangle$  and  $\langle I_y \rangle$  show an oscillatory behavior with time with frequency same as the Larmor frequency and  $\langle I_z \rangle$  is stationary. [8]

The eigenvalues associated with the Zeeman hamiltonian are proportional to the eigenvalues of the  $I_z$  operator. The energy levels in the nucleus are therefore given by:

$$E_m = -m\hbar\omega_L \quad (2.4)$$

The Nucleus with spin  $I$  is broken into  $2I+1$  equally spaced energy levels with higher  $m$  states having the lower energy. The ground state is the state where  $m = I$ , which in the semi-classical picture corresponds to the fact that the nucleus is as aligned as possible with the external magnetic field.

For an ensemble of identical nuclei in thermal equilibrium, the Boltzmann Distribution gives the population in each level. For the spin  $1/2$  case :

$$\frac{n_{m=-1/2}}{n_{m=+1/2}} = \exp\left\{\frac{-\hbar\omega_L}{k_B T}\right\} \quad (2.5)$$

where  $k_B$  is the Boltzman constant and  $T$  is the absolute temperature of the ensemble. Proceeding with the values of the quantities involved, we see that the population excess that provides net magnetization is very less about 1 in  $10^5$ , which is the reason behind the very low sensitivity of NMR experiments. This result can be naively interpreted as meaning that more nuclei are parallel than in the anti-parallel direction of the magnetic field. Semiclassically, we can view this net magnetization as a result of the Larmor precession. The nonvanishing  $z$  component remains while the transverse component gets canceled out because of the randomness of spin motion around the precession cone.[8]

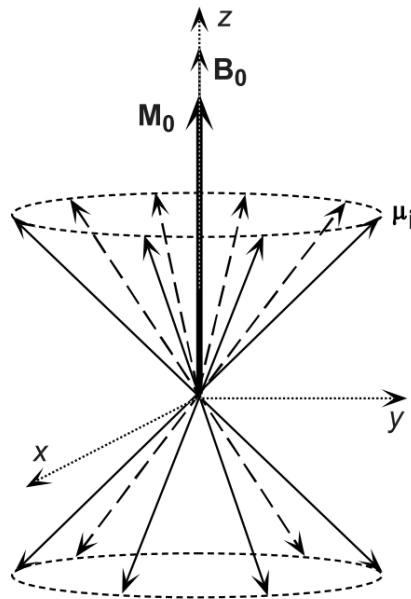


**Figure 2.2:** More spins precess around the direction parallel to field than against it, giving rise to net macroscopic magnetization which points in the direction of the field. [8]

## 2.3 Interaction with the Radio Frequency Field

The phenomenon of resonance is exploited for NMR applications. We can induce transitions between various energy levels with the help of oscillating magnetic fields with appropriate frequency. In case of NMR, Larmor frequencies are of the order of MHz for static fields of the order of few T. Hence the excitation is achieved by applying RF field. This can be understood in detail with the help of the following example. Take a field  $B_1(t)$ , which is applied perpendicular to the static field, say along x-direction. We can write  $B_1(t)$  as:

$$B_1(t) = 2B_1 \cos(\omega t + \phi) \mathbf{i} \quad (2.6)$$

where  $\omega$  and  $\phi$  are the frequency and phase of the RF field, respectively. The Hamiltonian for this can be written as:

$$H_{RF} = -\mu \cdot B_1(t) = -\gamma \hbar I_x [2B_1 \cos(\omega t + \phi)] \quad (2.7)$$

An important thing to note here is that the magnitude of  $B_1(t)$  is around few gauss, which is very small as compared to the magnitude of the static field applied and hence this hamiltonian can be treated as a perturbation to the Zeeman Hamiltonian. Proceeding ahead with the time-dependent perturbation theory, we get the result that when the frequency of the field is close to the Larmor frequency of the qubit, then we can drive transitions between the Zeeman sublevels, and the the rate of these transitions is governed by the Fermi Golden Rule:[8]

$$P_{a \rightarrow b} = P_{b \rightarrow a} \propto \gamma^2 \hbar^2 B_1^2 |\langle a | I_x | b \rangle|^2 \quad (2.8)$$

From the above equation we can clearly see that the transition rate grows with the square of the gyromagnetic ratio and the magnitude of the applied magnetic field. Also, it is evident that in order to maximize the probability of transition between the Zeeman states we need to apply the Rf pulse in the direction that is perpendicular to the direction of the static field. The properties of  $I_x$  (or  $I_y$ ) operator govern the transition rules for these transitions. The rule boils down to  $\Delta m = \pm 1$ . Besides this pure quantum mechanical treatment of the system, there also exists another semi classical description of the same which provides a way to visualize the dynamics of the spin. This description is known as vector model or the semi classical model.

### 2.3.1 Vector Model

The total Hamiltonian of the system is given as,

$$H_{total} = -\hbar \omega_L I_z - \gamma \hbar I_x [2B_1 \cos(\omega t + \phi)] \quad (2.9)$$

Now, the total magnetic field experienced by the spin is given as (assuming ideal conditions),

$$B_{total} = B_0 \mathbf{k} + 2B_1 \cos(\omega t + \phi) \mathbf{i} \quad (2.10)$$

To make visualization simple we assume the applied RF field to be linearly polarized along the x-axis. We can now decompose this field into two circularly polarized fields  $B_1^+(t)$  and  $B_1^-(t)$ , i.e.

$$B_1(t) = B_1^+(t) + B_1^-(t) \quad (2.11)$$

where the two fields are :

$$B_1^+(t) = B_1 [\cos(\omega t + \phi) \mathbf{i} + \sin(\omega t + \phi) \mathbf{j}] \quad (2.12)$$

$$B_1^-(t) = B_1 [\cos(\omega t + \phi) \mathbf{i} - \sin(\omega t + \phi) \mathbf{j}] \quad (2.13)$$

where  $B_1^-(t)$  rotates in anti-clockwise direction (precesses around the z-direction) and  $B_1^+(t)$  rotates in clockwise direction (precesses about -z direction).

Proceeding along the same lines we can clearly state the following points:

- $B_1^-(t)$  rotates coherently with the nuclear Larmor precession as described by the Equation.(2.2)
- $B_1^+(t)$  rotates in the opposite sense as that of the Larmor precession.

Now to avoid the trouble of having a time dependent rotation axis, consider shifting to the frame which is also rotating around the z-axis with a frequency  $\Omega = -\Omega \mathbf{k}$ . We call this frame the **Rotating frame**. In the Rotating frame,  $B_1^-(t)$  is static,  $B_1^+(t)$  is rotating about -z with frequency  $2\Omega$ , and the spin is rotating with the frequency  $(\omega_L - \Omega)$ .

To further simplify the analysis, we make the **Rotating wave approximation**. This approximation is generally used in atom optics and magnetic resonance. In this approximation, we neglect the terms the Hamiltonian which oscillate rapidly. This is a valid approximation as long as applied electromagnetic radiation is near resonance with an atomic transition, and the intensity is low.[8]

After applying the approximation the effective magnetic field reduces to (off resonance situation):

$$B_{eff} = (B_0 - \frac{\Omega}{\gamma_n}) \mathbf{k} + B_1 \mathbf{i}' \quad (2.14)$$

where  $\mathbf{i}'$  is the unit vector along the x-axis in the rotating frame and the resonance occurs when  $\omega_L = \Omega$ .

The effective Hamiltonian now reduces to :

$$H_{eff} = \omega_0 I_x + \omega_1 [\cos(\phi) I_x + \sin(\phi) I_y] \quad (2.15)$$

where  $\omega_0 = (\omega_L - \Omega)$  is called the offset frequency and  $\omega_1$  is called the **Nutation frequency**. Effectively the concept of rotating frame and rotating wave approximation has removed the time dependence from the hamiltonian and we can solve this using the Time Independent Schrodinger Equation.

### 2.3.2 Relation between lab and rotating frame

Consider two reference frames : Fixed reference frame (lab frame) with the axis  $x, y, z$  and the second being the rotating frame (about the  $z$  axis) with the axis  $x', y', z'$ . These two frames are related as,

$$x' = x \cos(\Phi(t)) - y \sin(\Phi(t)) \quad (2.16)$$

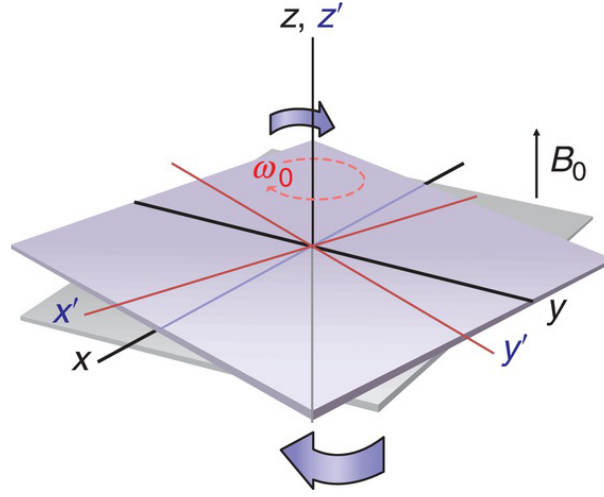


**Figure 2.3:** The rotating frame axis with reference to the lab frame ( $\omega_0 = \omega_{ref}$ ).

$$y' = y \cos(\Phi(t)) + x \sin(\Phi(t)) \quad (2.17)$$

where  $\Phi(t) = \omega_{ref} t + \phi$

## 2.4 Ensemble of spins

An ensemble is defined as a collection of identical and non-Interacting particles. The interactions between the particles with count of the order of Avagadro's Number can be neglected to a good approximation which means that we can consider that the particles do not influence each other and their collection can be treated as a good ensemble.

### 2.4.1 Concept of Density matrix

The most appropriate approach to describing NMR phenomena involves using the density matrix formalism from Quantum Statistical Mechanics. This approach is appropriate



because of large number of spins and no access to the individual quantum states of the particles, only to macroscopic averages. The density operator  $\rho$  of a collection of identical, independent nuclei (an ensemble) is defined in such a way that the macroscopic average of the expectation value of any observable  $A$  over the ensemble is given by :

$$\langle A \rangle = \text{Tr}[\rho A] \quad (2.18)$$

An important point to be kept in mind here is that the left-hand side is the statistical average over the entire ensemble and not the expectation value for a particular system in the ensemble. In thermal equilibrium, the concept of density matrix can be related to the Hamiltonian of the system :

$$\rho_0 = \frac{\exp\{-H/k_B T\}}{\sum_m \exp\{-E_m/k_B T\}} \quad (2.19)$$

Where sum is extended over all the eigenstates of the Hamiltonian and  $E_m$  represents the Eigenvalues of  $H$ . The sum in the denominator is called the partition function of the system.

In a given orthonormal basis, the density operator, just like other operators, has a matrix representation, which is called the density matrix :

$$\rho = \begin{pmatrix} \rho_{11} & \rho_{12} & \dots \\ \rho_{21} & \rho_{22} & \dots \\ \dots & \dots & \dots \end{pmatrix}$$

The density matrix of any ensemble satisfies some basic properties:

1. It is Hermitian
2. The diagonal elements are greater than or equal to zero.
3. The sum of these diagonal elements is equal to unity.

It is important to note here that it has some special properties because of its construction. The diagonal elements are called the populations, and the off-diagonal elements are called the coherences. This has a physical meaning to it. These values are related to the probability of finding a member of the ensemble in a given state when we perform a macroscopic measurement. The above-mentioned property number 3, therefore corresponds to the condition of normalization.[8]

In the basis of Hamiltonian eigenbasis, the thermal equilibrium density matrix can be written as:

$$\rho_0 = \begin{pmatrix} \exp\{-E_1/k_B T\} & 0 & \dots \\ 0 & \exp\{-E_2/k_B T\} & \dots \\ \dots & \dots & \dots \end{pmatrix}$$

This is a simple form of density matrix which shows that in thermal equilibrium, the population obey the Boltzmann distribution, whereas there are zero coherences.

For an ensemble of nuclei in the presence of identical nuclei under the Zeeman Hamiltonian and in the  $I_z$  basis, the population in thermal equilibrium are given by:

$$[\rho_0]_{mm} = \frac{\exp\{m\hbar\omega_L/k_B T\}}{\sum_{s=-I}^I \exp\{s\hbar\omega_L/k_B T\}} \quad (2.20)$$

In the high temperature limit, where the thermal energy is much greater than the Zeeman level spacing, we can use the following approximations :

$$\exp\{m\hbar\omega_L/k_B T\} \simeq 1 + \frac{m\hbar\omega_L}{k_B T} \quad (2.21)$$

$$\sum_{s=-I}^I \exp\{s\hbar\omega_L/k_B T\} \simeq 2I + 1 \quad (2.22)$$

Therefore, the thermal equilibrium density matrix for a system of identical nuclei in static magnetic field under the high temperature limit can be written as:

$$\rho_0 = \left(\frac{1}{2I+1}\right) \mathbf{I} + \left(\frac{1}{2I+1} \frac{\hbar\omega_L}{k_B T}\right) I_z \quad (2.23)$$

where  $\mathbf{I}$  is the identity matrix and is insensitive to NMR transformations and the second term is called the deviation matrix and will be used extensively in the next section.

## 2.5 The Theory of Relaxation

It is important to understand the concept of relaxation as it outlines several fundamental limitations to the spin systems. Stating it in the layman terms and on the basis of a purely logical statement, every system has the inherent tendency to revert back to its equilibrium/ ground state. So, everytime we excite a particular system, we need to take into consideration the time that the system takes to revert back to its original state and the harsh reality is every interesting feature offered by these systems in hand can be exploited only with the help of excited states and nothing happens if we leave the system in its ground state. We have to disturb the system, do the stuff and wait for the system to respond, while keeping in mind the system limitations of reverting back to the ground state. Same is the case with the NMR systems. Everytime we apply a pulse what we basically do is excite the system, e.g. take into consideration a simple  $90^\circ$  pulse applied to a system in the thermal equilibrium state. The pulse brings down the magnetization vector in the xy plane if we talk in the semi-classical picture or we can say it equalizes the population in both the ground and the excited state. According to the eq.(2.15), the evolution of the state is just the rotation of the magnetization vector about the z axis in

the xy plane. In the absence of any external field the system should continue to oscillate for infinite amount of time (semi-classical). But in reality what we detect is that the amplitude of the oscillation decreases with time and decays back to zero after a certain time span. This detection corresponds to the loss/disappearance of the net transverse magnetization and its conversion into the longitudinal magnetization, which means that the system starts coming back to its equilibrium state. This behaviour of the system is termed as **Relaxation**. To have a deeper look into the theory and to realize how this imposes fundamental restrictions we will look into the details of two types of relaxation processes that take place simultaneously :

- Longitudinal Relaxation
- Transverse Relaxation

### 2.5.1 Longitudinal Relaxation

Longitudinal Relaxation refers to the recovery of the z-component of the magnetization vector.

Talking in terms of energy levels, the thermal state has less energy as compared to the excited state, so as a result the excited system loses its energy to the nearby environment and relaxes back to the ground state and this is also commonly known as the **Spin-Lattice Relaxation**. We call the characteristic time scale associated with this as the  $T_1$  time scale. It is generally of the order of several seconds. The differential equation associated with the dynamics of the longitudinal magnetization vector is :

$$\frac{dM_z}{dt} = \frac{M_0 - M_z}{T_1} \quad (2.24)$$

which provides the following solution,

$$M_z = M_0(1 - e^{-\frac{t}{T_1}}) \quad (2.25)$$

Now, to experimentally measure the  $T_1$  time scale associated with the given sample, we apply the following pulse sequence :

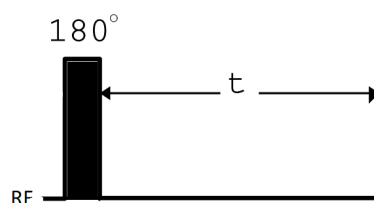


**Figure 2.4:** The pulse sequence used to measure the longitudinal relaxation.

The  $180^\circ$  pulse rotates the magnetization vector to the  $-z$  axis and we wait for the system to relax and return back to its original state and the time given to the system is mentioned as  $t$ . Since we can't perceive the magnetization along the  $z$ -axis, so we apply an additional  $90^\circ$  pulse which projects the spectra in the  $xy$  plane so that it can be visualized. After applying this pulse sequence we acquire the signal. We sweep through the time  $\tau$  and visualize the spectra till the maximum amplitude is obtained and the minimum time required for that provides the  $T_1$  time scale.

### 2.5.2 Transverse Relaxation

As explained in section (2.4.1), the off diagonal entries in the density operators represent the coherences present in the ensemble. The loss of coherence in the transverse magnetization, leads to disappearance of the transverse magnetization after the application of the rf pulse. This is known as **Transverse Relaxation** or **Spin-Spin relaxation**.

This loss of magnetization is caused by the spread of the Larmor frequencies of the spins present in the sample. If we refer to eq.(2.2), we can clearly see that this variation can only be caused by the variation in the magnetic field experienced by different spins. This variation in the net magnetic field experienced by the spins can be explained by taking into consideration the various nuclear spin-spin interaction present in the system. These interaction have been discussed in detail in the next section.

The dynamics of transverse magnetization are described by the following differential equation :

$$\frac{dM_{x,y}}{dt} = \frac{-M_{x,y}}{T_2} \quad (2.26)$$

which provides the following solution,

$$M_{x,y} = M_0(e^{-\frac{t}{T_2}}) \quad (2.27)$$

The  $T_2$  time scale of the system that is used for NMR quantum computing is generally of the order of few seconds but is always less than the  $T_1$  time scale mentioned earlier. So all the practical limitations are imposed by the  $T_2$  time scale. All the pulse duration combined should be well below the  $T_2$  time scale so that a signal of good quality can be recorded.

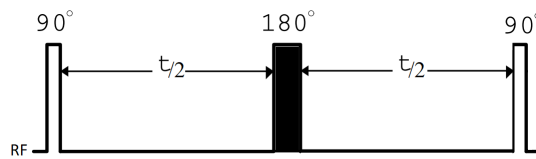


**Figure 2.5:** The pulse sequence used to measure the  $T_2$  time scale.

$T_2$  is typically measured using a spin echo pulse sequence. After superposition, local magnetic fields cause a phase accumulation during the first free precession interval  $\tau/2$ . However, when the local magnetic field fluctuations are slow on the time scale of the free precession interval  $\tau/2$ , the RF  $\pi$  pulse inverts the accumulated phase such that the same amount of phase is accumulated over the second free precession interval  $\tau/2$ , thus refocusing the net phase and ideally eliminating the net phase shift. The time is then swept and we record the amplitude values which are then fitted with the function described by eq.(2.27) to get the  $T_2$  value.

## 2.6 Important Nuclear Spin Interactions

Four types of interactions play an important role in NMR:

1. Chemical Shift
2. J-coupling
3. Dipolar Coupling
4. Quadrupolar Coupling

### 2.6.1 Chemical Shift

The nucleus is spatially surrounded by the other atoms in the molecules as well as an effective electron cloud which has its own magnetic field which interferes with the external magnetic field that we apply. As a result of this, the net magnetic field experienced by the nucleus becomes the vector sum of both the fields. So, the local magnetic field at the site of the nucleus can be written as:

$$B_{local} = (1 - \hat{\sigma})B_0 \quad (2.28)$$

where  $\hat{\sigma}$  is known as the chemical shielding vector for that particular site and its tensorial nature implies anisotropy of the molecular environment. To simplify the Hamiltonian, some assumptions are taken into account. We assume that the Zeeman interaction is much stronger than Chemical shift (secular approximation). The hamiltonian for the chemical shift interaction is therefore written as:

$$H_{CS} = -\gamma\hbar\sigma_{zz}B_0I_z \quad (2.29)$$

### 2.6.2 J-coupling

It is also known as **scalar coupling**. This interaction is mediated through chemical bonds. It is typically a weak interaction in comparison to the Zeeman interaction. It causes further

splitting in the peaks in the NMR spectrum. The interaction Hamiltonian associated with the J coupling is given by:

$$H_J = 2\pi\hbar I_1 \cdot \tilde{J} \cdot I_2 \quad (2.30)$$

J couplings can exist in both the homonuclear systems (e.g. between hydrogen with different chemical shifts) as well as in heteronuclear systems (e.g. between hydrogen and carbon).

### 2.6.3 Dipolar Coupling

Dipolar Coupling originates from the direct interaction through magnetic field generated by the magnetic dipoles. If we treat spin as a classical magnetic dipole then the magnetic field generated by it becomes:

$$B_{dipole} = \frac{\mu_0}{4\pi} \frac{3(\mu \cdot e)e - \mu}{r^3} \quad (2.31)$$

where  $\mu$  is the magnetic dipole moment,  $r$  is the magnitude or distance and  $e$  is the unit vector along  $r$ . The final interaction term is then given by:

$$H_{dipole} = \frac{\mu_0}{4\pi} \frac{\gamma_1 \gamma_2 \hbar^2}{r_{12}^3} [\mathbf{I}_1 \mathbf{I}_2 - 3(\mathbf{I}_1 \cdot \mathbf{e}_{12})(\mathbf{I}_2 \cdot \mathbf{e}_{12})] \quad (2.32)$$

### 2.6.4 Quadrupolar Coupling

This coupling appears in the case of nuclei that have spin value  $> \frac{1}{2}$ . This comes into play because of non spherical distribution of charge around such nuclei which gives rise to non-zero electric quadrupole moment. This moment then couples with the electric field gradient at the nuclear position and gives rise to the following interaction term:

$$H_{Quadrupolar} = \frac{e^2 q Q}{4I(2I-1)} [3I_z^2 - I^2 + \eta(I_x^2 - I_y^2)] \quad (2.33)$$

# Chapter 3

## Pseudo Pure State

### 3.1 Theory

As mentioned in the introductory chapters, the conventional NMR deals with a very large ensemble of spins because of extremely low population excess. This results in a state that is a statistical mixture making it inadequate for QIP. The production of a pure state is simply ruled out because of the principles of statistical mechanics. For performing the computation, we need to work with the well defined pure state. This problem was worked out by Cory et al.[13] and Chuang et al., which resulted in an important method for creating the so-called pseudo pure states.[3]

The important thing to note here is that the NMR experiments are sensitive only to the traceless deviation density matrices. Therefore they searched for transformations which need to be applied to the thermal equilibrium density matrices so that they produce a density matrix which closely resembles deviation density matrix corresponding to a pure state. Now an immediate thing that comes to mind when we talk about transformations in quantum mechanics is a Unitary transformation. So proceeding with this idea, let's define a state  $\rho' = U\rho U^\dagger$ . The aim is to examine if this state, with some unitary transformations applied to the thermal equilibrium state, resembles a pure state. Before proceeding ahead with this analysis, some important properties that we need to know are:

- The properties of density matrix corresponding to a pure state are :  $\rho = \rho^n$  and  $Tr(\rho^2) = 1$
- The properties of density matrix corresponding to a mixed state are :  $\rho \neq \rho^n$  and  $Tr(\rho^2) < 1$

Continuing with the same example we get:[10]

$$Tr(\rho'^2) = Tr([U\rho U^\dagger]^2) = Tr(U\rho U^\dagger U\rho U^\dagger) = Tr(U\rho^2 U^\dagger) = Tr(\rho^2) < 1 \quad (3.1)$$

$$\rho'^n = (U\rho U^\dagger)^n = \prod_{i=1}^n (U\rho U^\dagger) = U\rho^n U^\dagger \neq U\rho U^\dagger \neq \rho \quad (3.2)$$

This clearly shows that **it is impossible to obtain a pure state from a mixed state just by applying unitary operations**. Therefore, the creation must involve some non-unitary operation or some kind of averaging over different mixed states. There are many ways to perform such operations in NMR and a few of them which are popularly used are mentioned below:

- **Temporal Averaging:** In this technique a set of states are prepared by applying unitary transformations to a common initial state (usually a thermal equilibrium state), and they are then combined to produce an average state that behaves like a pure state.
- **Spatial Averaging:** In this technique, a system is divided into spatially separated sub-ensembles. These sub-ensembles can be accessed independently in NMR by applying various pulse and pulse gradients (equivalent to applying different unitary operations on different sub ensembles). The pseudo pure state is then achieved by averaging over all these ensembles.
- **State Labeling:** This method is a bit different from the ones mentioned above as it does not make use of sub-ensembles of spins or any averaging procedures. One qubit is used to label the state, and the others are put into the pseudo pure configuration.

## 3.2 Spatial Averaging

As mentioned above, this method is based on dividing the system into spatially separated sub-ensembles. In simple terms, we can consider the macroscopic sample as being constituted by a set of sub-ensembles, each one represented by a density matrix. A designed set of pulses ensures that the sub ensembles have the same distribution of populations but with different off-diagonal elements. Now we need to remove them so that the average state behaves like a pure state. For this purpose, the pulse gradients are used, and their purpose is to introduce a dephasing for the coherences associated with different spatial locations along the sample. Since this dephasing is proportional to the gradient strength, a high gradient strength pulse ensure that the coherences span the whole range from 0 to  $2\pi$  along the sample. Now since the non-diagonal elements go out of phase spanning the whole spectrum, this ensures that the average density matrix over a reasonable number of sub-ensemble looks exactly like that of a pure state.[10]



### 3.3 Sequence generated for 4 qubit system(Result)

Pulse set1

$$\left[ \arccos\left(\frac{1}{8}\right) \right]_y^1 \left[ \arccos\left(\frac{1}{4}\right) \right]_y^2 \left[ \frac{\pi}{3} \right]_y^4 \rightarrow [\textit{gradient}]$$

Pulse set2

$$\rightarrow \left[ \frac{\pi}{4} \right]_y^2 \rightarrow \left[ U\left(\frac{1}{2J_{12}}\right) \right] \rightarrow \left[ \frac{\pi}{4} \right]_x^2 \rightarrow [\textit{gradient}]$$

Pulse set3

$$\rightarrow \left[ \frac{\pi}{4} \right]_y^3 \rightarrow \left[ U\left(\frac{1}{2J_{13}}\right) \right] \rightarrow \left[ U\left(\frac{1}{2J_{23}}\right) \right] \rightarrow \left[ \frac{\pi}{4} \right]_y^3 \rightarrow [\textit{gradient}]$$

Pulse set4

$$\rightarrow \left[ \frac{\pi}{4} \right]_y^3 \rightarrow \left[ U\left(\frac{1}{2J}\right) \right] \rightarrow \left[ \frac{-\pi}{4} \right]_x^3 \rightarrow [\textit{gradient}]$$

Pulse set5

$$\rightarrow \left[ \frac{\pi}{4} \right]_y^4 \rightarrow \left[ U\left(\frac{1}{4J_{14}}\right) \right] \rightarrow \left[ U\left(\frac{1}{4J_{24}}\right) \right] \rightarrow \left[ \frac{\pi}{4} \right]_x^4 \rightarrow [\textit{gradient}]$$

Pulse set6

$$\rightarrow \left[ \frac{\pi}{4} \right]_y^3 \rightarrow \left[ U\left(\frac{1}{2J_{13}}\right) \right] \rightarrow \left[ \frac{\pi}{4} \right]_x^3 \rightarrow [\textit{gradient}]$$

Pulse set7

$$\rightarrow \left[ \frac{\pi}{4} \right]_y^4 \rightarrow \left[ U\left(\frac{1}{2J_{14}}\right) \right] \rightarrow \left[ U\left(\frac{1}{2J_{24}}\right) \right] \rightarrow \left[ \frac{\pi}{4} \right]_y^4 \rightarrow [\textit{gradient}]$$

The combination of pulse sequence mentioned above generates the following deviation density matrix:

$$\begin{pmatrix} 0.9375 & 0 & 0 & 0 & 0 & 0 & 0 & 0 & 0 & 0 & 0 & 0 & 0 \\ 0 & -0.0625 & 0 & 0 & 0 & 0 & 0 & 0 & 0 & 0 & 0 & 0 & 0 \\ 0 & 0 & -0.0625 & 0 & 0 & 0 & 0 & 0 & 0 & 0 & 0 & 0 & 0 \\ 0 & 0 & 0 & -0.0625 & 0 & 0 & 0 & 0 & 0 & 0 & 0 & 0 & 0 \\ 0 & 0 & 0 & 0 & -0.0625 & 0 & 0 & 0 & 0 & 0 & 0 & 0 & 0 \\ 0 & 0 & 0 & 0 & 0 & -0.0625 & 0 & 0 & 0 & 0 & 0 & 0 & 0 \\ 0 & 0 & 0 & 0 & 0 & 0 & -0.0625 & 0 & 0 & 0 & 0 & 0 & 0 \\ 0 & 0 & 0 & 0 & 0 & 0 & 0 & -0.0625 & 0 & 0 & 0 & 0 & 0 \\ 0 & 0 & 0 & 0 & 0 & 0 & 0 & 0 & -0.0625 & 0 & 0 & 0 & 0 \\ 0 & 0 & 0 & 0 & 0 & 0 & 0 & 0 & 0 & -0.0625 & 0 & 0 & 0 \\ 0 & 0 & 0 & 0 & 0 & 0 & 0 & 0 & 0 & 0 & -0.0625 & 0 & 0 \\ 0 & 0 & 0 & 0 & 0 & 0 & 0 & 0 & 0 & 0 & 0 & -0.0625 & 0 \\ 0 & 0 & 0 & 0 & 0 & 0 & 0 & 0 & 0 & 0 & 0 & 0 & -0.0625 \end{pmatrix}$$

The above deviation density matrix corresponds to a pure state of  $|0000\rangle$ . The theoretical proof for this can be found below.

### 3.4 Product Operator Analysis

The thermal equilibrium deviation density matrix for the four qubit system is given by :

$$I_z^1 + I_z^2 + I_z^3 + I_z^4$$

The analysis for the pulse sequence written above can be done as:

$$\begin{aligned}
 I_z^1 + I_z^2 + I_z^3 + I_z^4 &\xrightarrow{\text{Pulse set 1}} \frac{1}{8}I_z^1 + \frac{1}{4}I_z^2 + I_z^3 + \frac{1}{2}I_z^4 \\
 &\xrightarrow{\text{Pulse set 2}} \frac{1}{8}I_z^1 + \frac{1}{8}I_z^2 + I_z^3 + \frac{1}{2}I_z^4 + \frac{1}{4}I_z^1I_z^2 \\
 &\xrightarrow{\text{Pulse set 3}} \frac{1}{8}I_z^1 + \frac{1}{8}I_z^2 + \frac{1}{2}I_z^3 + \frac{1}{2}I_z^4 + \frac{1}{4}I_z^1I_z^2 + 2I_z^1I_z^2I_z^3 \\
 &\xrightarrow{\text{Pulse set 4}} \frac{1}{8}I_z^1 + \frac{1}{8}I_z^2 + \frac{1}{4}I_z^3 + \frac{1}{2}I_z^4 + \frac{1}{4}I_z^1I_z^2 + \frac{1}{2}I_z^3I_z^4 \\
 &\quad + I_z^1I_z^2I_z^3 + 2I_z^1I_z^2I_z^3I_z^4 \\
 &\xrightarrow{\text{Pulse set 5}} \frac{1}{8}I_z^1 + \frac{1}{8}I_z^2 + \frac{1}{4}I_z^3 + \frac{1}{4}I_z^4 + \frac{1}{4}I_z^1I_z^2 + \frac{1}{4}I_z^2I_z^4 \\
 &\quad + \frac{1}{4}I_z^3I_z^4 + I_z^1I_z^2I_z^3 + \frac{1}{2}I_z^1I_z^3I_z^4 + \frac{1}{2}I_z^2I_z^3I_z^4 + I_z^1I_z^2I_z^3I_z^4 \\
 &\xrightarrow{\text{Pulse set 6}} \frac{1}{8}I_z^1 + \frac{1}{8}I_z^2 + \frac{1}{8}I_z^3 + \frac{1}{4}I_z^4 + \frac{1}{4}I_z^1I_z^2 + \frac{1}{4}I_z^1I_z^3 \\
 &\quad + \frac{1}{4}I_z^1I_z^4 + \frac{1}{4}I_z^2I_z^3 + \frac{1}{4}I_z^2I_z^4 + \frac{1}{4}I_z^3I_z^4 + \frac{1}{2}I_z^1I_z^2I_z^3 \\
 &\quad + \frac{1}{2}I_z^1I_z^3I_z^4 + \frac{1}{2}I_z^2I_z^3I_z^4 + I_z^1I_z^2I_z^3I_z^4 \\
 &\xrightarrow{\text{Pulse set 7}} \frac{1}{8}I_z^1 + \frac{1}{8}I_z^2 + \frac{1}{8}I_z^3 + \frac{1}{8}I_z^4 + \frac{1}{4}I_z^1I_z^2 + \frac{1}{4}I_z^1I_z^3 \\
 &\quad + \frac{1}{4}I_z^1I_z^4 + \frac{1}{4}I_z^2I_z^3 + \frac{1}{4}I_z^2I_z^4 + \frac{1}{4}I_z^3I_z^4 + \frac{1}{2}I_z^1I_z^2I_z^3 \\
 &\quad + \frac{1}{2}I_z^1I_z^2I_z^4 + \frac{1}{2}I_z^1I_z^3I_z^4 + \frac{1}{2}I_z^2I_z^3I_z^4 + I_z^1I_z^2I_z^3I_z^4
 \end{aligned}$$

which is the pseudo pure state configuration for the four qubit system.

# Chapter 4

## Optimal Control Using GRAPE

### 4.1 Motivation

Traditionally NMR has been used to probe an unknown system, so most NMR experiments make use of the rectangular RF (hard) pulses which are very close to the Larmor Frequency of the qubits (or various nuclei present in the system). These pulses carry very high power levels for a very short duration of time (typically few  $\mu\text{s}$ ). Since they are rectangular in shape their power reaches to maximum with no time and holds on to that level for the entire specified duration and after that power immediately drops back to zero. These pulses work very well as long as we want to excite multiple qubits[7]. These pulses fail in case we want to perform selective excitation without disturbing the other qubits or without disturbing the neighbouring peaks of single qubit only. For this purpose NMR spectroscopists make use of the **soft pulses**. Soft (or shaped) pulses are employed for selective excitation of the spectral width. That means they can be used for exciting only specific portion of the entire spectrum. These pulses generally have long time periods and make use of minimal power levels so that the rest of spectrum stays undisturbed.

But to fully exploit the available experimental degrees of freedom and to realize the true potential of NMR systems, these pulses need to be tailored specifically for the system under consideration to get deeper insights and best possible results. This is where **Optimal Control Theory** comes into play. It was originally designed for optimization in the other fields like engineering, finance but has been extremely effective in designing pulses for systems having complicated internal Hamiltonians and large number of external parameters. It is capable of handling thousands of free variables within an optimization and provides the optimal solution way faster than the standard optimization techniques. In recent few years this dynamic theory has found its way into nuclear magnetic resonance as tool for efficient pulse design. This opens up the possibility of taking into account the system specific information like nucleus type, nuclear interaction sizes, RF inhomogeneities, bandwidth limitations and various other relevant parameters into account while designing the pulses for specific purposes.[16]

## 4.2 Optimal control in NMR

Diving into the very basics of NMR, the final aim is to apply the desired unitary operator, which is nothing but a combination of designed pulses. All we have is coils arranged in the x-y plane, that can be used to steer the magnetization in the desired direction. Now the current that we pass to these coils are the control knobs which can be adjusted, and the other parameter in hand is the total time of the pulse. Now, we breakdown the total time duration of the pulse into small time steps and we work with the assumption that the control knob values will remain constant for these time steps and can vary between different steps. Now for each qubit under consideration, there are 2 controls that we have i.e. the phase and amplitude of the pulse for each time step. Therefore a simple single qubit rotation unitary we have  $2 \times (\text{number of time steps})$  number of variables and the number of time steps is typically around 1000. All these variables are then used as input into the framework of Optimal control theory and the goal is to be able to generate the right pulse for the unitary. Some of the common methods used for pulse design are listed below:

- GRAPE
- KROTOV
- CRAB
- GOAT

Fig 4.1 shows which numerical optimization method is best for the situation in hand where  $J$  is the function to be minimized,  $n$  is the number of variables in hand,  $\epsilon(t)$  represents the control fields and  $\phi_k$  represent the states.

## 4.3 Theory of GRAPE

### 4.3.1 Transfer between Hermitian operators

The state of the spin system is demarcated by its density operator  $\rho(t)$ . The dynamics for the same is governed by the Liouville-von Neumann Equation (which can be derived directly from the Schrodinger Equation)

$$\dot{\rho}(t) = -i \left[ \left( H_0 + \sum_{k=1}^m u_k(t) H_k \right), \rho(t) \right] \quad (4.1)$$

Here  $H_0$  is the free evolution Hamiltonian which contains the offset error terms as well as the coupling term,  $H_k$ 's are the radio-frequency (rf) Hamiltonians corresponding to the control fields that are available, and  $u(t) = u_1(t), u_2(t), \dots, u_m(t)$ , represent the control

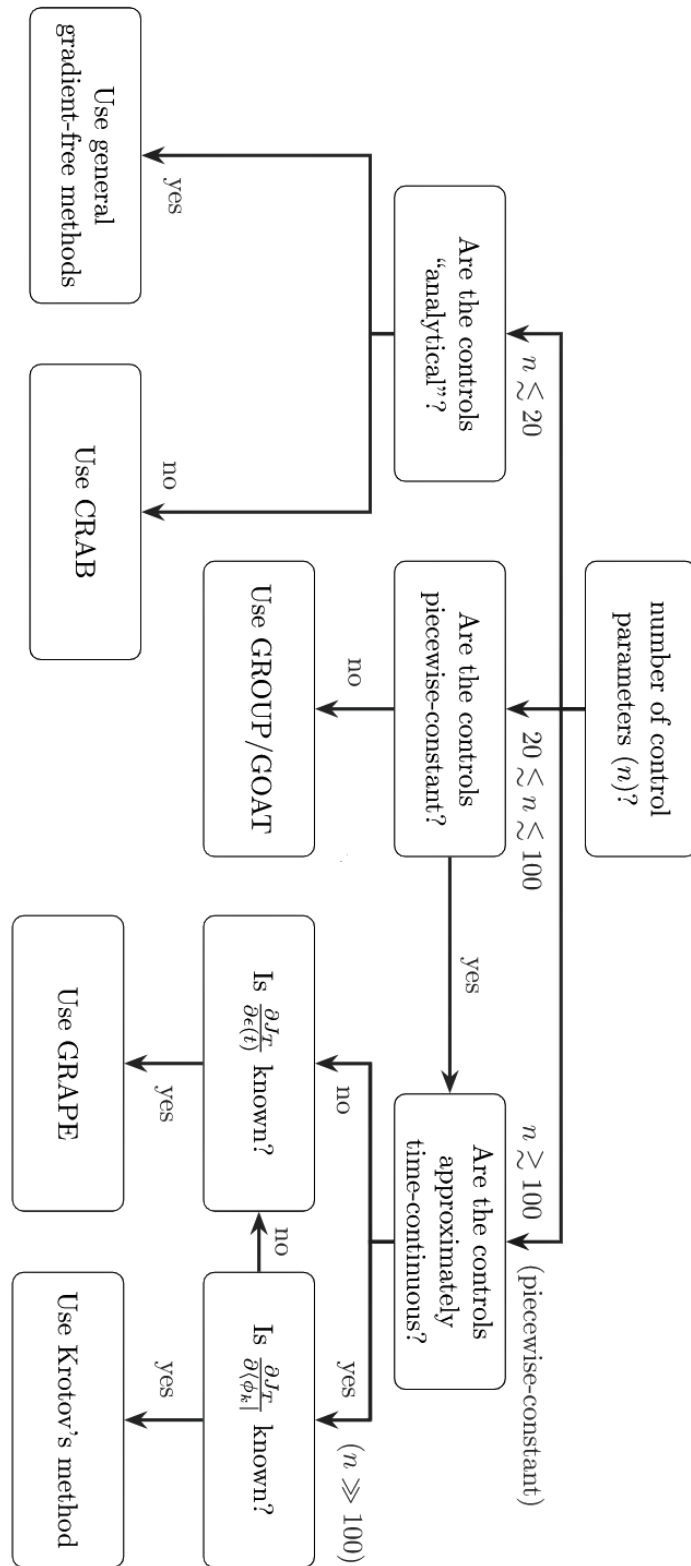


**Figure 4.1:** Decision flow chart for choice of numerical optimization method. [4]

vectors(to control the magnitude of the field that is applied for driving transitions between the Zeeman sub-levels). The aim is to find optimal amplitudes  $u_k(t)$  of the control fields

so that the given initial density operator  $\rho(0) = \rho_0$  in a given time  $T$  can be changed into a density operator  $\rho(T)$  which has maximum overlap with the target operator  $C$ . For the Hermitian operators this overlap is defined by the standard inner product.

$$\langle C | \rho(T) \rangle = \text{tr}[C^\dagger \rho(T)] \quad (4.2)$$

Hence we can define the performance index  $\phi_0$  required in the Optimal Control Theory as:

$$\phi_0 = \langle C | \rho(T) \rangle \quad (4.3)$$

For simplicity, assumption that we will now make is that the total transfer time  $T$  can be discretized into  $N$  equal steps and for the duration of each time step  $\Delta t = T/N$  the control amplitudes  $u_k$  remain constant. This means that the control amplitude  $u_k(t)$  is given by  $u_k(j)$ . Now the time evolution of system during the time step  $j$  is given by the propagator:

$$U_j = \exp\{-i\Delta t \left( H_0 + \sum_{k=1}^m u_k(j) H_k \right)\} \quad (4.4)$$

Therefore the density operator at time  $t=T$  can be written as:

$$\rho(T) = U_N \dots U_1 \rho_0 U_1^\dagger \dots U_N^\dagger. \quad (4.5)$$

And the performance function can therefore be written as:[5]

$$\phi_0 = \langle C | U_N \dots U_1 \rho_0 U_1^\dagger \dots U_N^\dagger \rangle \quad (4.6)$$

Using the cyclic invariance of trace and the properties of inner product we can re-write this as:

$$\phi_0 = \langle U_{j+1}^\dagger \dots U_N^\dagger C U_N \dots U_{j+1} | U_j \dots U_1 \rho_0 U_1^\dagger \dots U_j^\dagger \rangle = \langle \lambda_j | \rho_j \rangle \quad (4.7)$$

where  $\rho_j$  represents the density operator  $\rho(t)$  at time  $t = j\Delta t$  and the  $\lambda_j$  is the backward propagated target operator  $C$  at the same time. Now focusing on the changes in the performance index when we add perturbation to the control amplitudes at time step  $j$ . From Eqn (4.4) we can see that the change to  $U_j$  to first order in  $\delta u_k(j)$  is given by :[5]

$$\delta U_j = -i\Delta t \delta u_k(j) H'_k U_j \quad (4.8)$$

where

$$H'_k \Delta t = \int_0^{\Delta t} U_j(\tau) H_k U_j(-\tau) d\tau \quad (4.9)$$

Moving ahead with the assumption that  $\Delta t$  is small, we can take  $H'_k \approx H_k$  and using Eqn(4.7) and Eqn(4.8) we can write:

$$\frac{\delta \phi_0}{\delta u_k(j)} = -\langle \lambda_j | i\Delta t [H_k, \rho_j] \rangle \quad (4.10)$$

So to increase the performance function we choose[5]

$$u_k(j) \longrightarrow u_k(j) + \epsilon \frac{\delta \phi_0}{\delta u_k(j)} \quad (4.11)$$

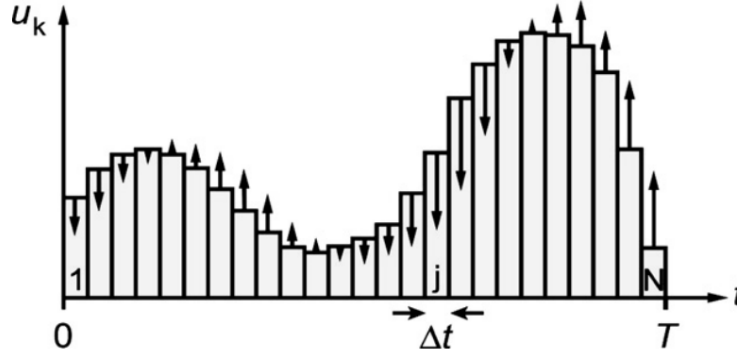


**Figure 4.2:** Schematic representation of a control amplitude  $u_k(t)$ , consisting of  $N$  steps of equal duration  $\Delta t$ . The Vertical arrows represent respective gradients indicating how each amplitude should be modified in the next iteration to improve the performance function under consideration.[5]

### 4.3.2 Synthesis of Unitary Transformations

We can define a similar problem to create a desired unitary operator in a given time  $T$ . The equation of motion for the propagator can therefore be written as (assuming that we are working with a closed quantum system)[6]

$$U\dot{(t)} = -i \left( H_0 + \sum_{k=1}^m u_k(t) H_k \right) U \quad (4.12)$$

At time  $t=0$  we can simply consider the propagator to be identity.

Now we consider the problem of approaching a desired propagator  $U_f$  by applying a pulse sequence  $u_j(t)$  so that after time  $T$ [5]

$$\|U_f - U(T)\|^2 = \|U_f\|^2 - 2\text{Re}\langle U_f | U(T) \rangle + \|U(T)\|^2 \quad (4.13)$$

is minimized, which means we need to maximize  $\text{Re}\langle U_f | U(T) \rangle$ . Hence like the previous problem we can define the performance function as[1]

$$\phi = \text{Re}\langle U_f | U(T) \rangle \quad (4.14)$$

$$= \text{Re}\langle U_f | U_N \dots U_1 \rangle \quad (4.15)$$

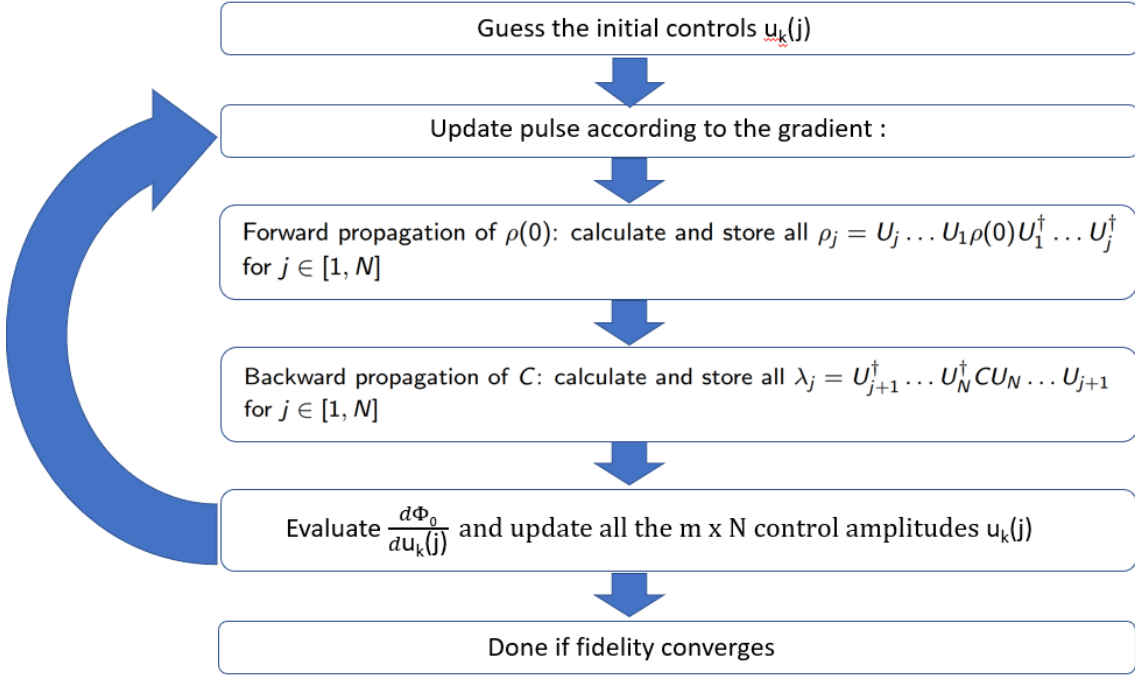
$$= \text{Re}\langle U_{j+1}^\dagger \dots U_N^\dagger U_f | U_j \dots U_1 \rangle \quad (4.16)$$



The algorithm to be concerned remains the same. Just the update in the pulse vector controls changes to

$$\frac{\delta\phi}{\delta u_k(j)} = -\text{Re} \left\langle U_{j+1}^\dagger \dots U_N^\dagger U_F \middle| i\Delta t H_k U_j \dots U_1 \right\rangle \quad (4.17)$$

## 4.4 Basic Algorithm



## 4.5 Features of the code written

I have included certain special features to the code that help me achieve these high fidelities and make sure that Pulse design can be directly implemented on the machine without post processing to make sure that the controls are within the machine limits.

### 4.5.1 Robustness against offset error

The free evolution part of the hamiltonian ( $H_0$ ) contains the offset term along with the coupling term. The offset term added to the hamiltonian of the form[2]

$$H_{offset} = -\hbar(offset1)I_z \quad (4.18)$$

This term is added for each qubit in the system. This makes sure that pulse design already incorporates the fact that the RF field applied by the machine is not exactly in synchronization with the Larmor frequency of the qubit in the applied static field.

### 4.5.2 Robustness against RF Miscalibration

This error occurs because of in-homogeneity in the control field generated by the NMR probe/coil.

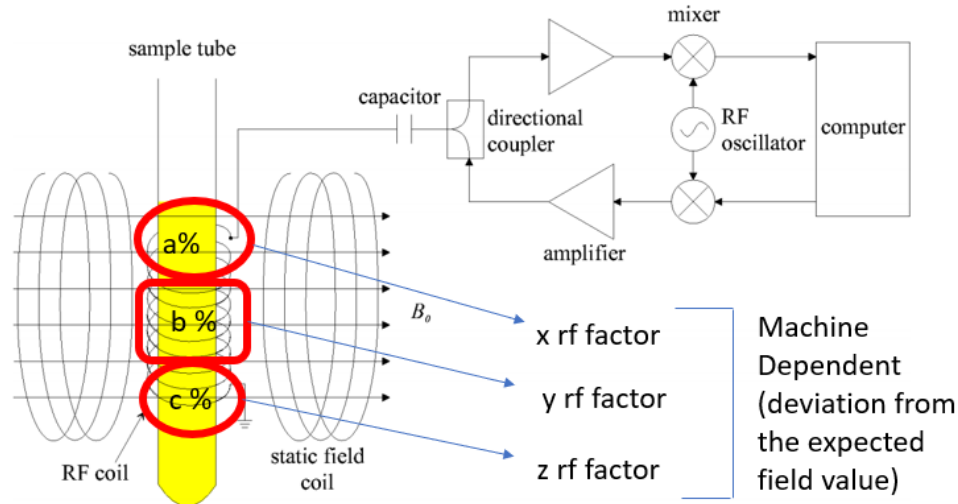


**Figure 4.3:** Schematic representation of NMR and with effective field value parameters

Fig(4.3) shows the schematic of NMR where x,y,z are the effective field values and a,b,c are the proportion of total sample that is exposed to the corresponding effective field. This was tackled by considering this as three different sub-systems. The code runs thrice by taking the factors into account one by one. The derivative is calculated using all three values and the value of the control field is updated by multiplying the correction terms with the percent of sample facing that particular rf field value.

### 4.5.3 Reduction of RF Power

This was incorporated easily into the above listed formalism by adding an additional penalty term to the performance function. This is done to ensure minimum heating of the sample and to ensure the demanded power stays well within the machine limits. This additional term reflects directly in the gradient calculation.[11]

$$\frac{\delta \phi}{\delta u_k(j)} = -2\alpha u_k(j)\Delta t. \quad (4.19)$$

where  $\alpha$  is the weight of the penalty imposed for using excess RF power.

### 4.5.4 Smooth Initial and Final controls

Another important feature added to the code was that of smooth end controls. This was done to ensure that the machine doesn't start or end with high power values causing

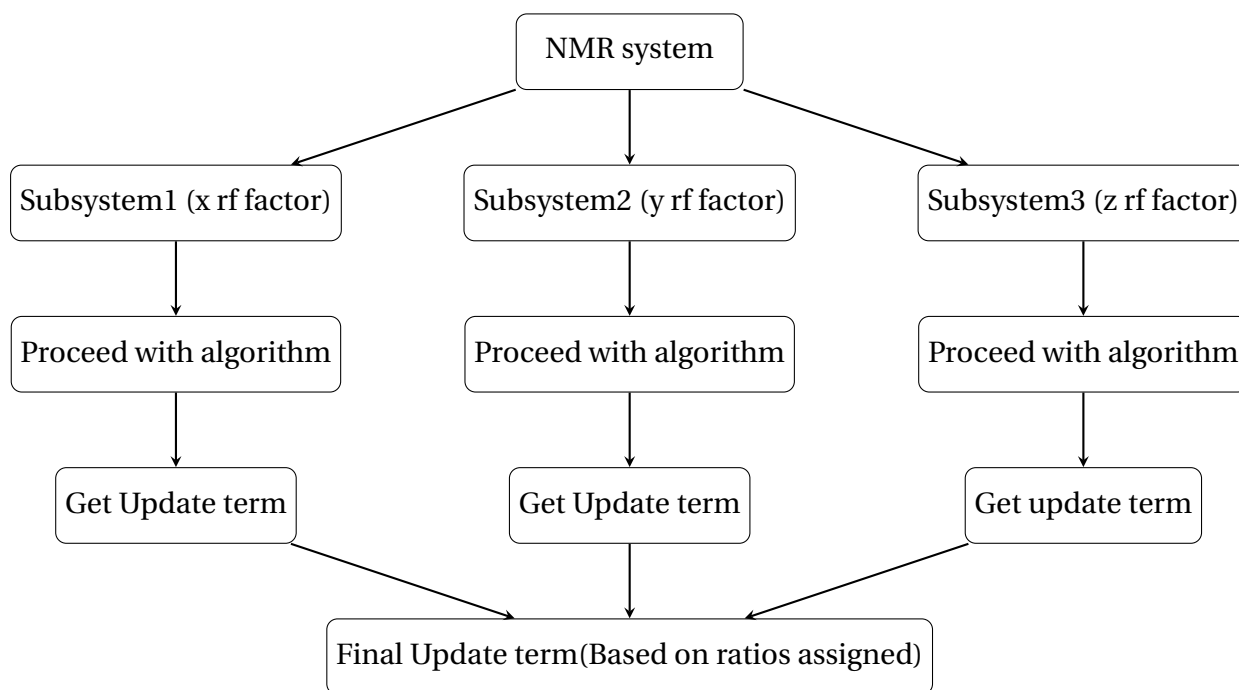


**Figure 4.4:** The above tree diagram represents how each loop proceeds to incorporate the RF miscalibration error.

damage to the electronics. Also, sudden implication of high power makes computing prone to errors because of the limitations of the electronics involved.

## 4.6 Bandwidth Control

The design of system specific pulses seems easy theoretically, the real problem kicks in when we try to apply these pulses on the NMR machine. One of the most under-represented problem in case of optimal control of NMR systems is the problem of **Phase transients** which have a significant impact on the NMR experiments, even the pulses with high theoretical fidelities fail to deliver the expected results. This is because of abrupt changes in amplitude and phase values of the numerically optimized pulses which result in high frequency pulses which often go out the system bandwidth limitations resulting in large deviations from the ideal pulse shape.[15]

There are several solutions to this problem and I have listed some of them below :

- The most logical solution is to model the resonant probe circuit by taking into consideration the linear elements like capacitors, resistors and inductors. With the help of the elements, an impulse response can be calculated which can be used to model the actual field experienced by the sample for any particular input. Based on the difference between the expected and the generated signal, the GRAPE algorithm

can be modified to take practicalities into account. This solution is logical but requires precise description of the system model and has other limitations like it can not capture transient effects beyond the sampling frequency which is governed by the length of the time step.

- Another solution is based on basic electronics. Since the transient effects are because of the abrupt changes which essentially boil down to presence of high frequency components in the generated signal. These frequency components can be filtered out with the application of a low pass filter. This can be achieved by adding an additional term in the derivative calculation step of the GRAPE algorithm.

While the above listed solutions work perfect for solving the problem, but they tremendously slow down the numerical optimization process. So to circumvent the problem of slow computation, the code uses a different idea which is based on the essence of the above listed ideas.

The idea is that even though the NMR machine can take discrete values at a very fast time scale, its rare that these many points will be required to find a high fidelity pulse. Therefore the following strategy was applied :

- Find a high fidelity pulse with relatively large time steps (around 20  $\mu$ s). This length of the time step is dictated by the assumption considered in Eqn. 4.4. This high fidelity pulse doesn't consider any restriction on the high frequency values.
- This pulse can then be digitally smoothed(for details refer to Appendix B) keeping system frequency bandwidth in consideration.
- This pulse can be optimized using the same optimizer by feeding this as the guess pulse. Usually, there is very small loss of fidelity through this process and this can be quickly optimized back to high fidelity values.
- The above stated procedure can be repeated again if any required condition is not met.

# Chapter 5

## Results Obtained

### 5.1 Two Qubit System Description

The two qubit Experiments were performed on the two protons of the cytosine molecule. The two-qubit molecular structure, system parameters and the initial thermal states are shown in the Fig. 5.1 and Fig. 5.2

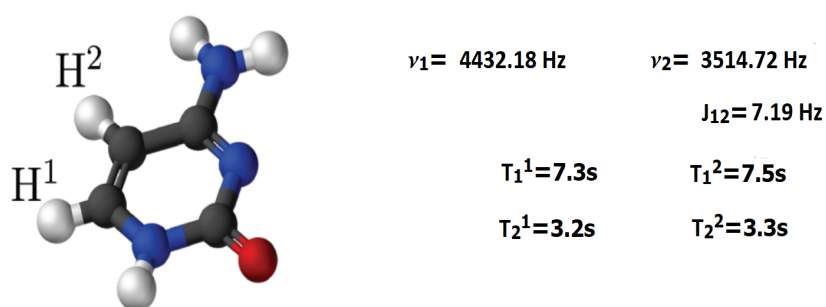


**Figure 5.1:** Molecular structure of cytosine with the two qubits labeled as  $H^1$  and  $H^2$  and the system parameters with chemical shifts  $\nu_i$ , coupling  $J_{12}$  (in Hz) and relaxation times  $T_1$  and  $T_2$  (in seconds).[14]

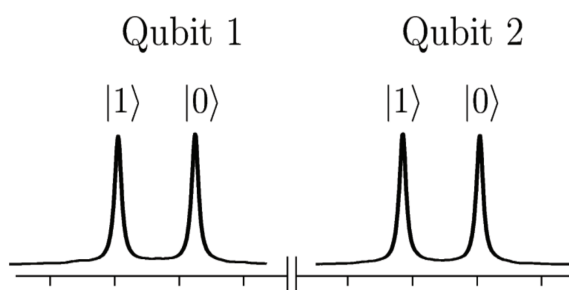


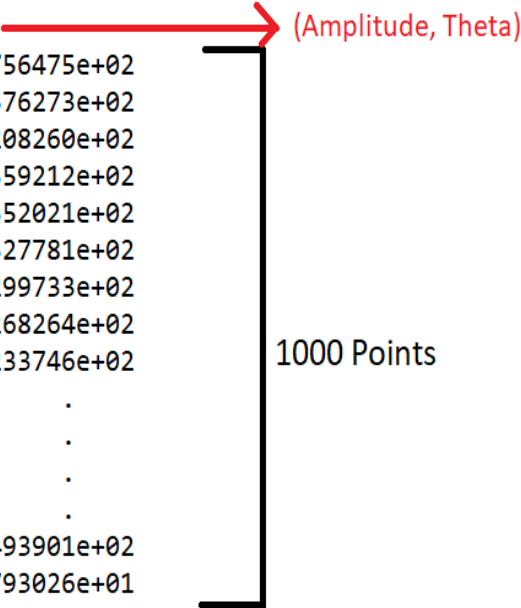
**Figure 5.2:** NMR spectrum obtained after a  $\pi/2$  rotation pulse on the thermal equilibrium state.

## 5.2 Output File

```

##TITLE= Cytosine_Q1_60x
##JCAMP-DX= 5.00 Bruker JCAMP library
##DATA TYPE= Shape Data
##ORIGIN= Saksham's GRAPE PULSE
##OWNER= SAKSHAM
##DATE= 07-Apr-2021
##TIME= 18:20
##MINX= 2.006710e-02
##MAXX= 1.109260e+02
##MINY= 6.240962e-02
##MAXY= 3.597228e+02
##$SHAPE_EXMODE= None
##$SHAPE_TOTROT= 0.000000e+01
##$SHAPE_BWFAC= 1.000000e+00
##$SHAPE_INTEGFAC= 1.000000e+00
##$SHAPE_MODE= 1
##NPOINTS= 1000
##XYPOINTS= (XY..XY)
    2.578894e-01, 1.756475e+02
    1.516146e-01, 1.576273e+02
    1.085602e+00, 1.208260e+02
    5.077781e+01, 1.359212e+02
    9.634051e+01, 1.352021e+02
    9.023599e+01, 1.327781e+02
    8.424634e+01, 1.299733e+02
    7.843398e+01, 1.268264e+02
    7.284944e+01, 1.233746e+02
    .
    .
    .
    .
    4.162370e-02, 3.493901e+02
    8.410385e-02, 7.793026e+01
##END=

```



(Amplitude, Theta)

1000 Points

**Figure 5.3:** This file contains the information about the amplitude and direction of the transverse magnetic field to be applied at every time step.

## 5.3 Single Qubit Rotations

As mentioned in section 3.1 one of the major benefits of using shaped pulses is that we can perform selective excitations. Here are some of the results obtained by selective rotation of qubits.

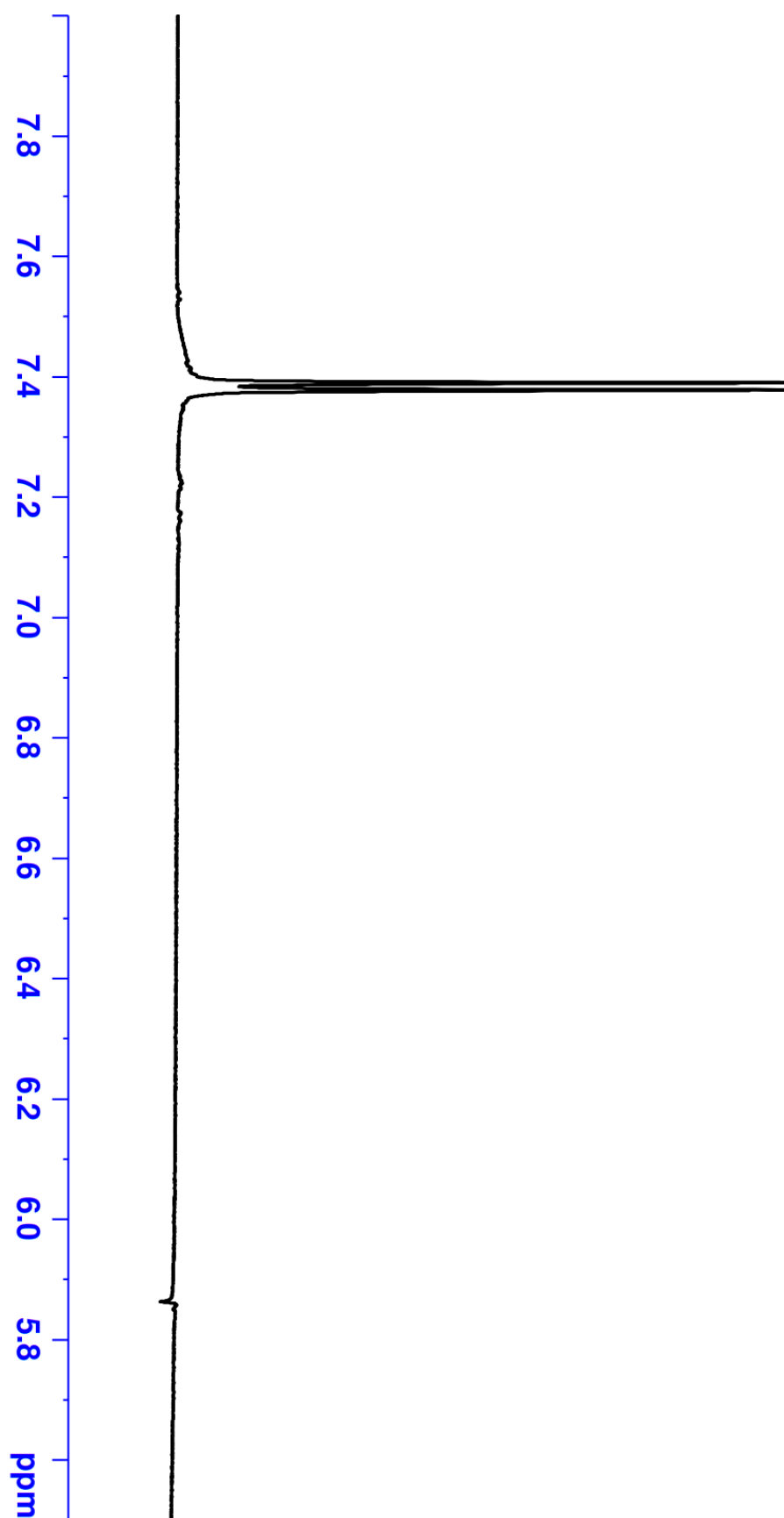


**Figure 5.4:** *Selective  $\pi/2$  rotation of qubit 1.*

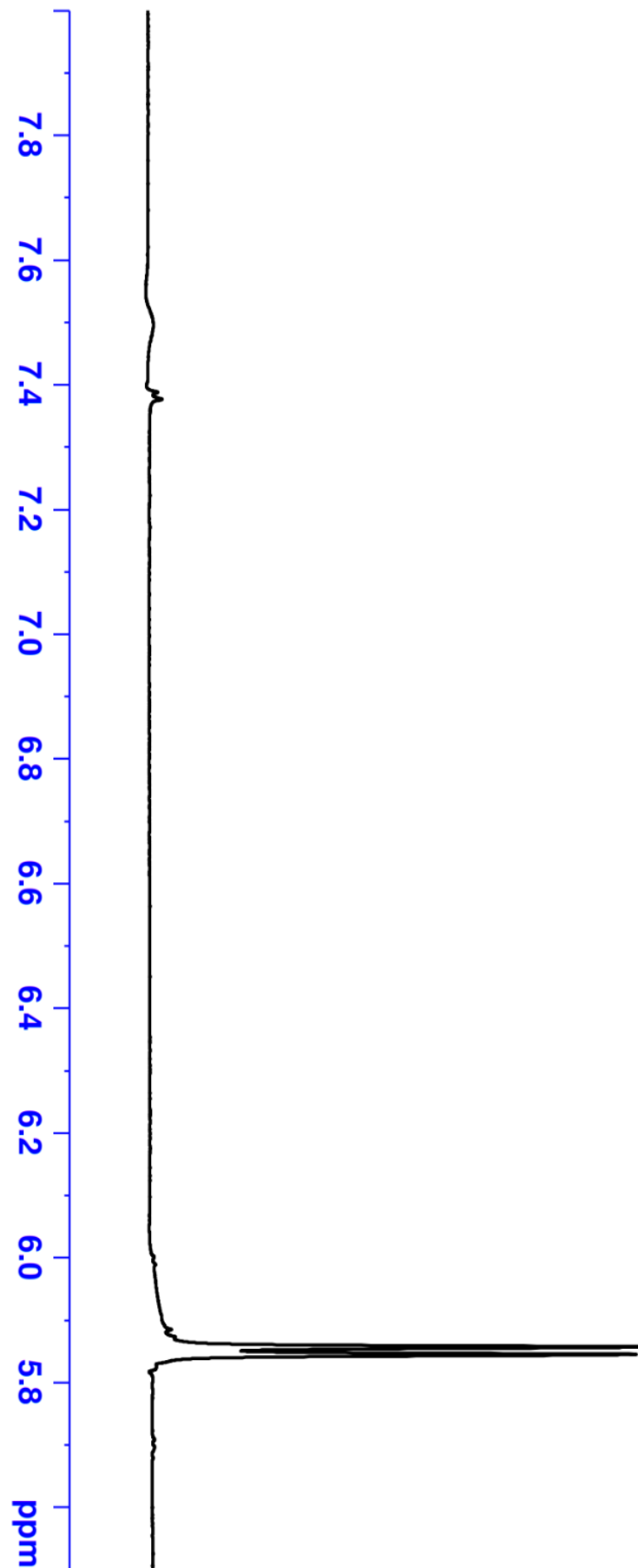


**Figure 5.5:** *Selective  $\pi/2$  rotation of qubit 2.*



## 5.4 Two Qubit Pseudo pure state

As mentioned in chapter 3, we need a well defined initial state for quantum computation and the thermal state is inadequate for the same. Therefore the following pulse sequence was used to convert two qubit thermal state into pseudo pure state.

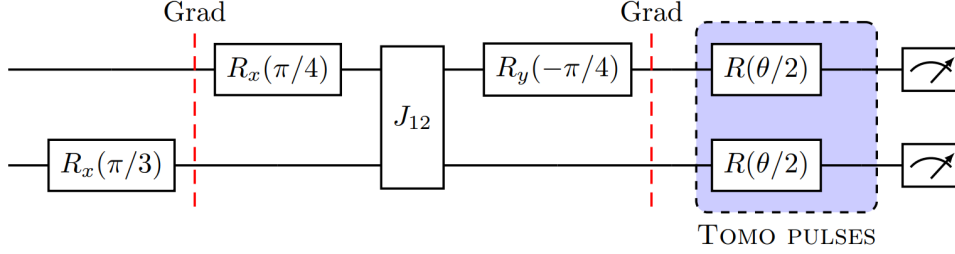


**Figure 5.6:** Quantum circuit for creating two qubit pseudo pure state.

In the above diagram, Grad stands for the gradient pulse which is a non-unitary operation. It destroys all the transverse magnetization while preserving the longitudinal component.  $J_{12}$  stands for free evolution under the J coupling. The product operator analysis of the above pulses sequence is done below:

The thermal equilibrium deviation density matrix for the two qubit system is given by:

$$I_z^1 + I_z^2$$

where  $I_z^1 = I_z \otimes I$  and  $I_z^2 = I \otimes I_z$

$$\begin{aligned}
 I_z^1 + I_z^2 &\xrightarrow{\left[\frac{\pi}{3}\right]_x} I_z^1 + \frac{1}{2}I_z^2 + \frac{\sqrt{3}}{2}I_x^2 \\
 I_z^1 + \frac{1}{2}I_z^2 + \frac{\sqrt{3}}{2}I_x^2 &\xrightarrow{\text{gradient}} I_z^1 + \frac{1}{2}I_z^2 \\
 I_z^1 + \frac{1}{2}I_z^2 &\xrightarrow{\left[\frac{\pi}{4}\right]_x} \frac{1}{\sqrt{2}}I_z^1 - \frac{1}{\sqrt{2}}I_y^1 + \frac{1}{2}I_z^2 \\
 \frac{1}{\sqrt{2}}I_z^1 - \frac{1}{\sqrt{2}}I_y^1 + \frac{1}{2}I_z^2 &\xrightarrow{\left[U\left(\frac{1}{2J}\right)\right]} \frac{1}{\sqrt{2}}I_z^1 + \frac{2}{\sqrt{2}}I_x^1I_z^2 + \frac{1}{2}I_z^2 \\
 \frac{1}{\sqrt{2}}I_z^1 + \frac{2}{\sqrt{2}}I_x^1I_z^2 + \frac{1}{2}I_z^2 &\xrightarrow{\left[\frac{\pi}{4}\right]_{-y}} -\frac{1}{2}I_x^1 + \frac{1}{2}I_z^1 + I_z^1I_z^2 + \frac{1}{2}I_z^2 \\
 -\frac{1}{2}I_x^1 + \frac{1}{2}I_z^1 + I_z^1I_z^2 + \frac{1}{2}I_z^2 &\xrightarrow{\text{gradient}} \frac{1}{2}I_z^1 + I_z^1I_z^2 + \frac{1}{2}I_z^2
 \end{aligned}$$

where  $\frac{1}{2}I_z^1 + I_z^1 I_z^2 + \frac{1}{2}I_z^2$  represents the pseudo pure state in a two qubit system.

The deviation density matrix obtained after applying the sequence mentioned is:

$$\rho_{deviation} = \begin{pmatrix} 0.75 & 0 & 0 & 0 \\ 0 & -0.25 & 0 & 0 \\ 0 & 0 & -0.25 & 0 \\ 0 & 0 & 0 & -0.25 \end{pmatrix} \quad (5.1)$$

As mentioned in Appendix A, we need 4 different tomography pulses in order to completely verify the state obtained. The pulses that are used for this purpose are II, IX, IY, XX

The result obtained after applying the II tomography pulse is given in Fig. 5.7. The result is in accordance with the matrix given by equation 5.1. (for details information provided by spectrum see Appendix A)

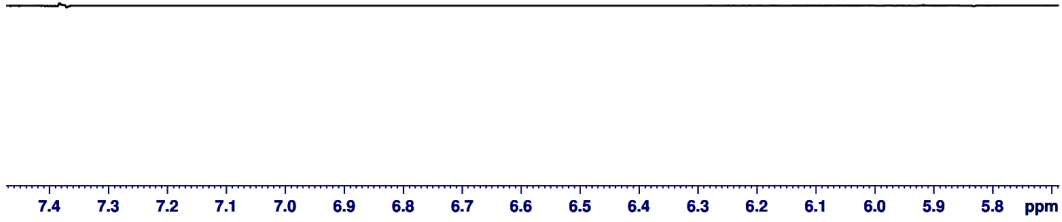


**Figure 5.7:** PPS spectrum after II tomography pulse.

When we apply IX pulse the density matrix changes to

$$\rho_{deviation} = \begin{pmatrix} 0.25 & 0.5\iota & 0 & 0 \\ -0.5\iota & 0.25 & 0 & 0 \\ 0 & 0 & -0.25 & 0 \\ 0 & 0 & 0 & -0.25 \end{pmatrix}$$

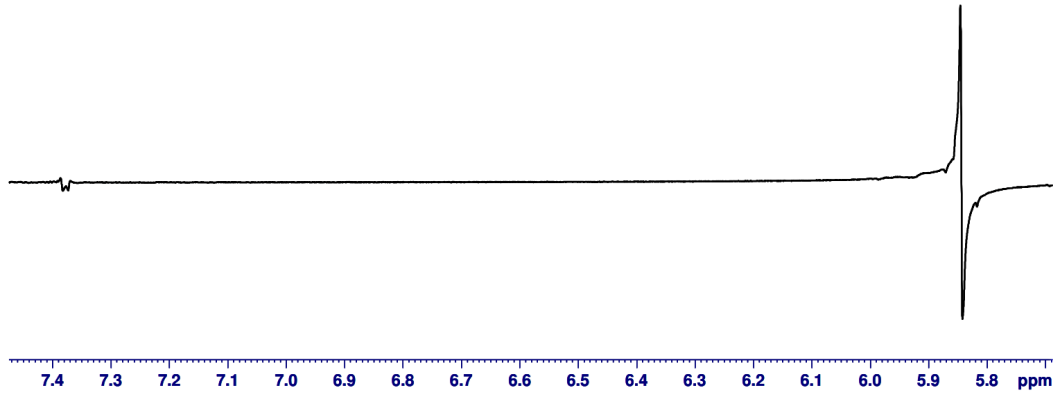


**Figure 5.8:** PPS spectrum after IX tomography pulse.

Similarly after applying IY pulse the density matrix changes to:

$$\rho_{deviation} = \begin{pmatrix} 0.25 & 0.5 & 0 & 0 \\ 0.5 & 0.25 & 0 & 0 \\ 0 & 0 & -0.25 & 0 \\ 0 & 0 & 0 & -0.25 \end{pmatrix}$$

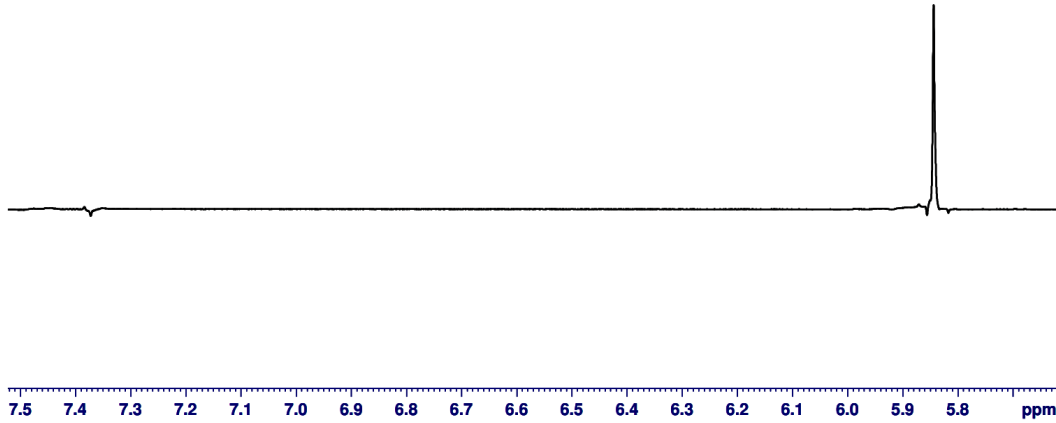


**Figure 5.9:** PPS spectrum after IY tomography pulse.

Finally, after applying XX pulse the density matrix changes to:

$$\rho_{deviation} = \begin{pmatrix} 0 & 0.25t & 0.25t & -0.25 \\ -0.25t & 0 & 0.25 & 0.25t \\ -0.25t & 0.25 & 0 & 0.25t \\ -0.25 & -0.25t & -0.25t & 0 \end{pmatrix}$$

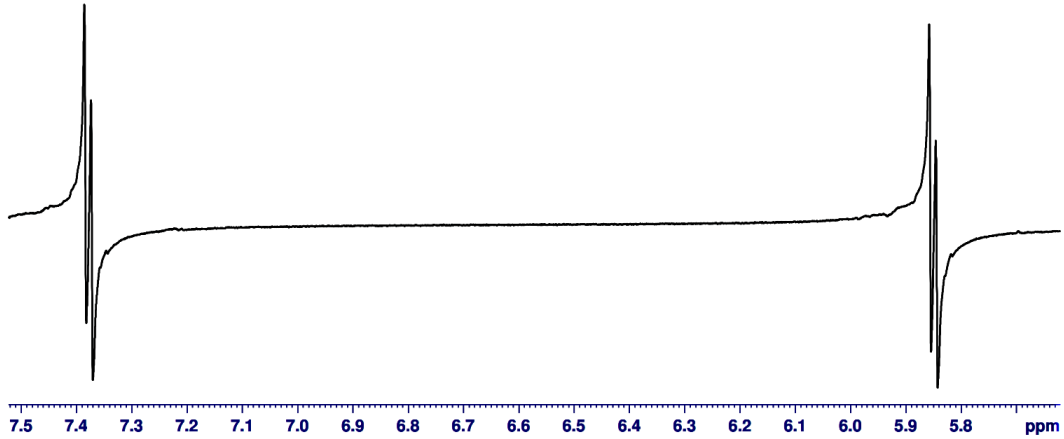


**Figure 5.10:** PPS spectrum after XX tomography pulse.

All four spectrum images (figures 5.7, 5.8, 5.9, 5.10) along with the stated theoretical density matrix values confirm the formation of pseudo pure  $|00\rangle$  state.

## 5.5 Quantum State Tomography

It is a standard method to reconstruct ensemble density matrix.

The following steps are followed to tomograph a state:

1. The real value of the density matrix element at any of the accessible positions is given by the area under the absorption spectrum and the imaginary part of the value is obtained after calculating the area under the spectrum after  $90^\circ$  phase shift.
2. Since all elements of density matrix are not directly accessible, we apply a set of RF pulses to permute the elements of the density matrix so that the above step can be repeated for those elements also.
3. Both the steps 1 and 2 are repeated till each element in the density matrix has been to the readout position.
4. For a two-qubit system the combination of RF pulses required are II, IX, IY and XX RF pulses.
5. After application of all the tomographic pulses, we get a series of linear equations.
6. Solve these linear equations to calculate all the density matrix values.

The most general 2 qubit deviation density matrix is given by(Hermitian):

$$\rho_{deviation} = \begin{pmatrix} a_{11} & a_{12} + \imath b_{12} & a_{13} + \imath b_{13} & a_{14} + \imath b_{14} \\ a_{12} - \imath b_{12} & a_{22} & a_{23} + \imath b_{23} & a_{24} + \imath b_{24} \\ a_{13} - \imath b_{13} & a_{23} - \imath b_{23} & a_{33} & a_{34} + \imath b_{34} \\ a_{14} - \imath b_{14} & a_{24} - \imath b_{24} & a_{34} - \imath b_{34} & a_{44} \end{pmatrix}$$

General analysis of the information available: In a homo-nuclear system, we have 4 bit of information available from one spectrum with two bit corresponding to each spin. The spectrum part corresponding to spin  $I_1$  depends only on the elements  $a_{13} + \imath b_{13}$  and  $a_{24} + \imath b_{24}$  and the spectrum corresponding to the spin  $I_2$  depends on  $a_{12} + \imath b_{12}$  and  $a_{34} + \imath b_{34}$ .

After we apply all the RF pulses in sequence and obtain the spectrum, integrating the area under the spectrum provides a series of linear equations by comparing the matrix elements to the area under the spectrum.

The equations can be written in the form:

$$A\vec{x} = \vec{y} \quad (5.2)$$

where A is 33 x 16 matrix,  $\vec{x}$  is 16 x 1 column matrix and  $\vec{y}$  is 33 x 1 column matrix with the values being determined by the area under the spectrum. Each homo nuclear spectrum provides 4 different linear equations (2 corresponding to each spin) and the 90 degree phase shifted spectrum provides another 4 equations. This means we get a total of 8 equations from one set of tomography pulses which then totals to 32 equations (because we use 4 tomography pulses) and we have one last trace preserving condition which takes the number of equations to 33. So overall we have 33 linear equations and 16 variables for 2 qubit system. Out of these 33 equations, 16 are linearly independent. To reduce the number of equations, we multiply eqn. 5.2 by  $A^T$ .

$$A^T A \vec{x} = A^T \vec{y} \quad (5.3)$$

the calculations were performed using mathematica.

$$\vec{x}^T = (a_{11} \quad a_{12} \quad b_{12} \quad a_{13} \quad b_{13} \quad a_{14} \quad b_{14} \quad a_{22} \quad a_{23} \quad b_{23} \quad a_{24} \quad b_{24} \quad a_{33} \quad a_{34} \quad b_{34} \quad a_{44})$$

$$M = A^T A = \begin{pmatrix} 2 & 0 & 0 & 0 & 0 & 0 & 0 & \frac{1}{2} & 0 & 0 & 0 & 0 & \frac{3}{2} & 0 & 0 \\ 0 & \frac{5}{2} & 0 & 0 & 0 & 0 & 0 & 0 & 0 & 0 & 0 & 0 & 0 & \frac{1}{2} & 0 \\ 0 & 0 & \frac{5}{2} & 0 & 0 & 0 & 0 & 0 & 0 & 0 & 0 & 0 & 0 & 0 & -\frac{1}{2} \\ 0 & 0 & 0 & \frac{5}{2} & 0 & 0 & 0 & 0 & 0 & 0 & \frac{3}{2} & 0 & 0 & 0 & 0 \\ 0 & 0 & 0 & 0 & \frac{5}{2} & 0 & 0 & 0 & 0 & 0 & 0 & \frac{1}{2} & 0 & 0 & 0 \\ 0 & 0 & 0 & 0 & 0 & 1 & 0 & 0 & 0 & 0 & 0 & 0 & 0 & 0 & 0 \\ 0 & 0 & 0 & 0 & 0 & 0 & 2 & 0 & 0 & 0 & 0 & 0 & 0 & 0 & 0 \\ \frac{1}{2} & 0 & 0 & 0 & 0 & 0 & 0 & \frac{3}{2} & 0 & 0 & 0 & 0 & 1 & 0 & 0 \\ 0 & 0 & 0 & 0 & 0 & 0 & 0 & 0 & 1 & 0 & 0 & 0 & 0 & 0 & 0 \\ 0 & 0 & 0 & 0 & 0 & 0 & 0 & 0 & 0 & 2 & 0 & 0 & 0 & 0 & 0 \\ 0 & 0 & 0 & \frac{3}{2} & 0 & 0 & 0 & 0 & 0 & 0 & \frac{5}{2} & 0 & 0 & 0 & 0 \\ 0 & 0 & 0 & 0 & \frac{1}{2} & 0 & 0 & 0 & 0 & 0 & 0 & \frac{5}{2} & 0 & 0 & 0 \\ \frac{3}{2} & 0 & 0 & 0 & 0 & 0 & 0 & 1 & 0 & 0 & 0 & 0 & \frac{5}{2} & 0 & 0 \\ 0 & \frac{1}{2} & 0 & 0 & 0 & 0 & 0 & 0 & 0 & 0 & 0 & 0 & 0 & \frac{5}{2} & 0 \\ 0 & 0 & -\frac{1}{2} & 0 & 0 & 0 & 0 & 0 & 0 & 0 & 0 & 0 & 0 & 0 & \frac{5}{2} \end{pmatrix}$$

$$M^{-1} = \begin{pmatrix} \frac{11}{12} & 0 & 0 & 0 & 0 & 0 & 0 & \frac{1}{12} & 0 & 0 & 0 & 0 & -\frac{7}{12} & 0 & 0 \\ 0 & \frac{5}{12} & 0 & 0 & 0 & 0 & 0 & 0 & 0 & 0 & 0 & 0 & 0 & -\frac{1}{12} & 0 \\ 0 & 0 & \frac{5}{12} & 0 & 0 & 0 & 0 & 0 & 0 & 0 & 0 & 0 & 0 & 0 & \frac{1}{12} \\ 0 & 0 & 0 & \frac{5}{8} & 0 & 0 & 0 & 0 & 0 & 0 & -\frac{3}{8} & 0 & 0 & 0 & 0 \\ 0 & 0 & 0 & 0 & \frac{5}{12} & 0 & 0 & 0 & 0 & 0 & 0 & -\frac{1}{12} & 0 & 0 & 0 \\ 0 & 0 & 0 & 0 & 0 & 1 & 0 & 0 & 0 & 0 & 0 & 0 & 0 & 0 & 0 \\ 0 & 0 & 0 & 0 & 0 & 0 & \frac{1}{2} & 0 & 0 & 0 & 0 & 0 & 0 & 0 & 0 \\ \frac{1}{12} & 0 & 0 & 0 & 0 & 0 & 0 & \frac{11}{12} & 0 & 0 & 0 & 0 & -\frac{5}{12} & 0 & 0 \\ 0 & 0 & 0 & 0 & 0 & 0 & 0 & 0 & 1 & 0 & 0 & 0 & 0 & 0 & 0 \\ 0 & 0 & 0 & 0 & 0 & 0 & 0 & 0 & 0 & \frac{1}{2} & 0 & 0 & 0 & 0 & 0 \\ 0 & 0 & 0 & -\frac{3}{8} & 0 & 0 & 0 & 0 & 0 & 0 & \frac{5}{8} & 0 & 0 & 0 & 0 \\ 0 & 0 & 0 & 0 & -\frac{1}{12} & 0 & 0 & 0 & 0 & 0 & 0 & \frac{5}{12} & 0 & 0 & 0 \\ -\frac{7}{12} & 0 & 0 & 0 & 0 & 0 & 0 & -\frac{5}{12} & 0 & 0 & 0 & 0 & \frac{11}{12} & 0 & 0 \\ 0 & -\frac{1}{12} & 0 & 0 & 0 & 0 & 0 & 0 & 0 & 0 & 0 & 0 & 0 & \frac{5}{12} & 0 \\ 0 & 0 & \frac{1}{12} & 0 & 0 & 0 & 0 & 0 & 0 & 0 & 0 & 0 & 0 & 0 & \frac{5}{12} \end{pmatrix}$$

Now,

$$\vec{x} = M^{-1} A^T \vec{y} \quad (5.4)$$

Since, we know  $M^{-1}$ ,  $A^T$  and  $\vec{y}$ , this gives us  $\vec{x}$  and hence the experimental density matrix.

The experimental deviation density matrix obtained for the pseudo pure state was:

$$\begin{pmatrix} 0.754 & 0.106 + 0.056i & -0.009 + 0.024i & -0.004 + 0.066i \\ 0.106 - 0.056i & -0.246 & 0.026 - 0.089i & 0.007 - 0.019i \\ -0.009 - 0.024i & 0.026 + 0.089i & -0.231 & 0.155 - 0.078i \\ -0.004 - 0.066i & 0.007 + 0.019i & 0.155 + 0.078i & -0.277 \end{pmatrix}$$

This provides the experimental fidelity of 0.945633 by using the fidelity measure defined in [17]

## 5.6 X-gate

X-gate is also known as bit flip gate and is one the most common single qubit gate. The unitary corresponding to this gate is

$$X = \begin{pmatrix} 0 & 1 \\ 1 & 0 \end{pmatrix} \quad (5.5)$$

In context of a two qubit system, It converts  $|00\rangle$  to  $|10\rangle$ ,  $|01\rangle$  to  $|11\rangle$ ,  $|10\rangle$  to  $|00\rangle$  and  $|11\rangle$  to  $|01\rangle$ .

$$X|00\rangle = \begin{pmatrix} 0 & 0 & 1 & 0 \\ 0 & 0 & 0 & 1 \\ 1 & 0 & 0 & 0 \\ 0 & 1 & 0 & 0 \end{pmatrix} \begin{pmatrix} 1 \\ 0 \\ 0 \\ 0 \end{pmatrix} = \begin{pmatrix} 0 \\ 0 \\ 1 \\ 0 \end{pmatrix} = |10\rangle \quad (5.6)$$

$$X|01\rangle = \begin{pmatrix} 0 & 0 & 1 & 0 \\ 0 & 0 & 0 & 1 \\ 1 & 0 & 0 & 0 \\ 0 & 1 & 0 & 0 \end{pmatrix} \begin{pmatrix} 0 \\ 1 \\ 0 \\ 0 \end{pmatrix} = \begin{pmatrix} 0 \\ 1 \\ 0 \\ 0 \end{pmatrix} = |11\rangle \quad (5.7)$$

$$X|10\rangle = \begin{pmatrix} 0 & 0 & 1 & 0 \\ 0 & 0 & 0 & 1 \\ 1 & 0 & 0 & 0 \\ 0 & 1 & 0 & 0 \end{pmatrix} \begin{pmatrix} 0 \\ 0 \\ 1 \\ 0 \end{pmatrix} = \begin{pmatrix} 1 \\ 0 \\ 0 \\ 0 \end{pmatrix} = |00\rangle \quad (5.8)$$

$$X|11\rangle = \begin{pmatrix} 0 & 0 & 1 & 0 \\ 0 & 0 & 0 & 1 \\ 1 & 0 & 0 & 0 \\ 0 & 1 & 0 & 0 \end{pmatrix} \begin{pmatrix} 0 \\ 1 \\ 0 \\ 1 \end{pmatrix} = \begin{pmatrix} 0 \\ 1 \\ 0 \\ 0 \end{pmatrix} = |01\rangle \quad (5.9)$$

This gate was applied to the pseudo pure 00 state. The resulting density matrix is

$$X\rho_{00}X^\dagger = \begin{pmatrix} -0.25 & 0 & 0 & 0 \\ 0 & -0.25 & 0 & 0 \\ 0 & 0 & 0.75 & 0 \\ 0 & 1 & 0 & -0.25 \end{pmatrix} \quad (5.10)$$

The spectrum obtained corresponding to the above density matrix was

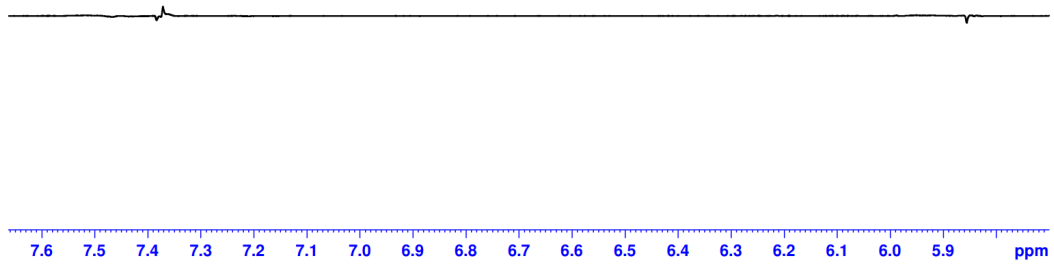


**Figure 5.11:** *X-gate spectrum after II tomography pulse.*

After applying the IX pulse the density matrix changes to

$$\begin{pmatrix} -0.25 & 0 & 0 & 0 \\ 0 & -0.25 & 0 & 0 \\ 0 & 0 & 0.25 & 0.5I \\ 0 & 0 & -0.5I & 0.25 \end{pmatrix} \quad (5.11)$$

The spectrum obtained after IX pulse is in agreement with the to the above density matrix

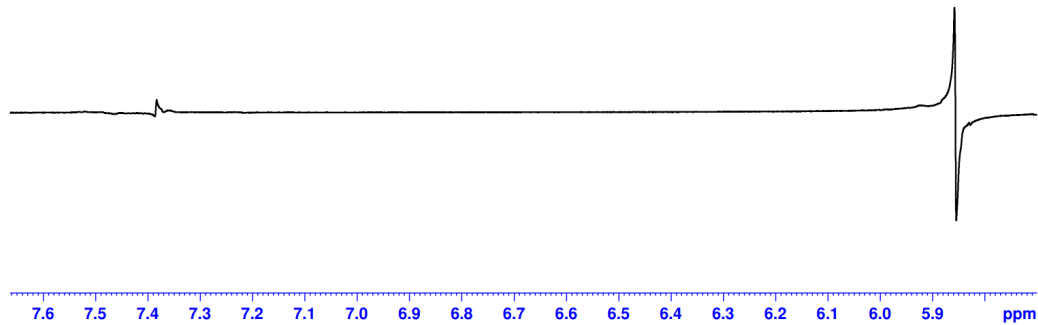


**Figure 5.12:** *X-gate spectrum after IX tomography pulse.*

After the IY pulse the density matrix becomes

$$\begin{pmatrix} -0.25 & 0 & 0 & 0 \\ 0 & -0.25 & 0 & 0 \\ 0.5 & 0 & 0.25 & 0.5 \\ 0 & 0 & 0.5 & 0.25 \end{pmatrix} \quad (5.12)$$

The spectrum obtained after IY pulse is in agreement with the to the above density matrix



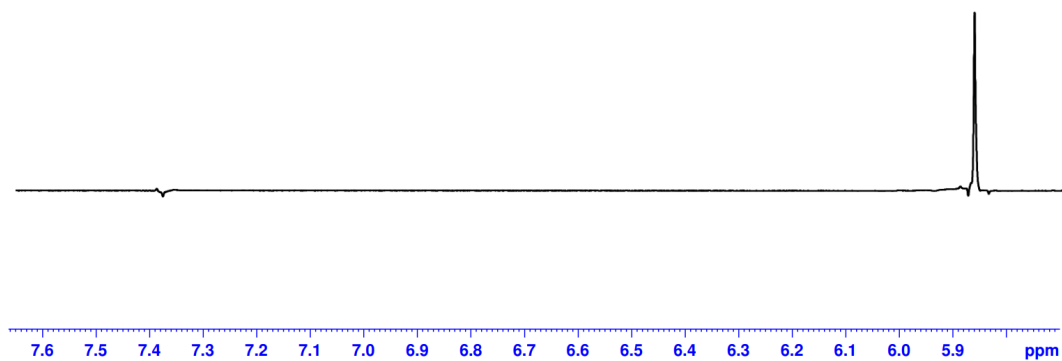


**Figure 5.13:** *X-gate spectrum after IY tomography pulse.*

After the XX pulse the density matrix becomes

$$\begin{pmatrix} 0 & 0.25\iota & -0.25\iota & 0.25 \\ -0.25\iota & 0 & -0.25 & -0.25\iota \\ 0.25\iota & -0.25 & 0 & 0.25\iota \\ 0.25 & 0.25\iota & -0.25\iota & 0 \end{pmatrix} \quad (5.13)$$

The spectrum obtained after XX pulse is in agreement with the to the above density matrix

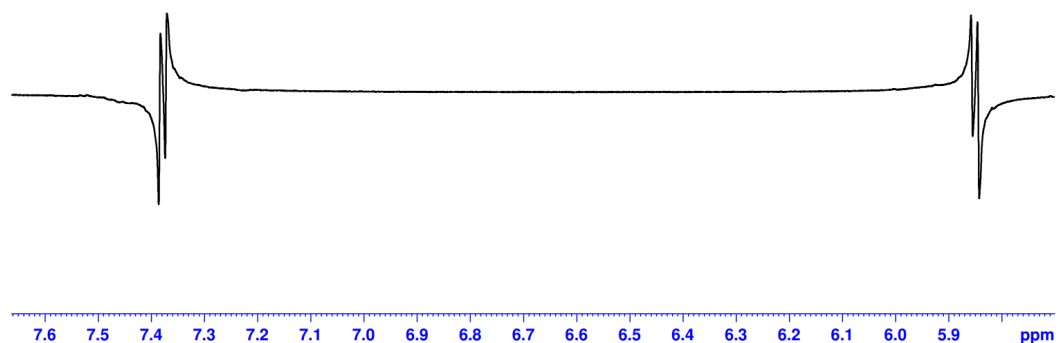


**Figure 5.14:** *X-gate spectrum after XX tomography pulse.*

# Chapter 6

## Summary and Conclusion

Chapter 1 successfully defines the motivation behind this thesis work. Chapter 2 provides a brief overview of the basic concepts required to understand the idea of NMR Quantum Computing. Chapter 3 provides theoretical overview of the Pseudo pure states and their importance in NMR Quantum Computing. The chapter also provides the sequence that can be used to create a pseudo pure state on a four qubit system and its theoretical proof. Chapter 4 outlines the basics of GRAPE, the method used for numerical optimization of pulses in this thesis. It also provides an insight into the extra features added to the code for implementing numerically optimized pulses on machine. Finally, Chapter 5 states all the results obtained by using numerically optimized pulses.

Numerically optimized GRAPE pulses were successfully developed and implemented jointly with the self written code and thesis code by Colm A. Ryan [12].

### 6.1 Tasks Completed

- Sequence for generating pseudo pure state in a 4 qubit system was successfully developed.
- Selective excitation of qubits in cytosine molecule was successfully carried out.
- Pseudo pure state was successfully prepared with spatial averaging method on a two qubit system.
- Bit-Flip gate was successfully implemented after creating the pseudo pure state.
- State tomography was successfully done to calculate the experimental fidelity of the pseudo pure state obtained.

### 6.2 Future Scope

- With some specific modification, the code can work with higher qubit systems.

- Also the implementation can be extended to hetero-nuclear systems.
- The precise measurement of RF distribution will help in reduction of experimental errors.

The use of GRAPE optimized pulses can open up doors for working with complex Unitary operators which can't be implemented by breaking down to simpler ones. It can also save the hustle to finding and applying the right set of RF pulses for any target unitary. In short this project holds in reserve a lot of potential which if properly exploited can open access of various under explored areas in NMR Quantum Computing,

# Appendix A

## Spectrum Information

In case of NMR system, we can read out only specific elements of the deviation density matrix at any particular time. The following diagram shows which elements of the deviation density matrix can be read and their corresponding peaks.

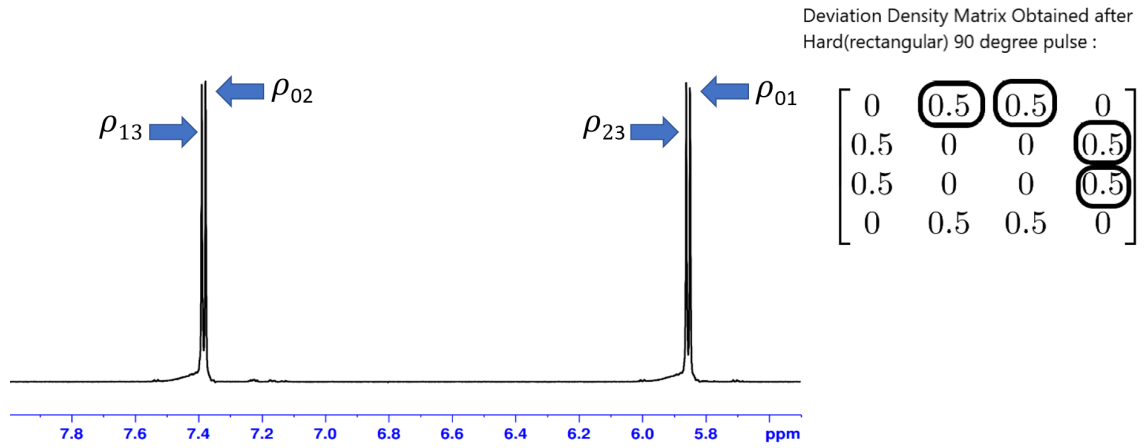


**Figure A.1:** Spectrum and deviation density matrix obtained after hard  $\pi/2$  pulses.

Since, two qubit density matrix has 16 elements and only 4 of them can be read, therefore, in order to completely verify the state a combination of four pulses: II, IX, IY, XX is required. These tomography pulses shift the elements of the deviation density matrix to these specific places so that their values can be verified.

# Appendix B

## Interpolation and Filtering

### B.1 Convolution Theorem

Convolution is very important technique in Digital Signal Processing. It is a mathematical framework to combine two different signals and generate a third signal. There is an important mathematical theorem Known as **convolution theorem**, which states that under suitable conditions the convolution of two functions is the point-wise product of Fourier transform of those functions. In context of the code, this theorem was used to keep bandwidth of generated pulse sequence in check. To state this in even simple terms, the convolution of two signals is equivalent to the product of the Fourier transforms of those function in the frequency domain. This technique was used to generate the suitable function to carry out interpolation of generated wave form.

### B.2 Ideal Low pass filter

Low pass filters are used in electronics to filter out the high frequencies i.e. frequencies above a pre-defined threshold. The frequency response of an ideal low pass filter is given in Fig. B.1. If we multiply this response of the ideal low pass filter with the output of the code then that ensures that the bandwidth of the signal will remain within machine constraints, This translates to convolution of Sinc function(inverse Fourier transform of ideal low pass filter function)(within suitable range) and the code generated output. The signal is then re-sampled at desired time steps and passed on the optimizer for Re-optimization.

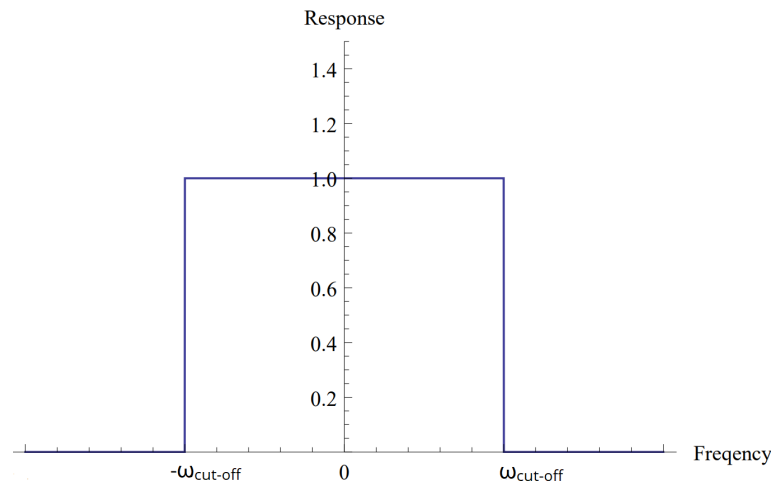


**Figure B.1:** *Frequency response of ideal low pass filter*

In some cases, this interpolation can turn out to be unstable. In such cases, the interpolation is done by taking Gaussian envelope and interpolating the signal using techniques such as cubic spline.

# Bibliography

- [1] Gaurav Bhole and Jonathan A. Jones. Practical pulse engineering: Gradient ascent without matrix exponentiation. *Frontiers of Physics*, 13(3):130312, May 2018.
- [2] Amit Devra, Prithviraj Prabhu, Harpreet Singh, Arvind, and Kavita Dorai. Efficient experimental design of high-fidelity three-qubit quantum gates via genetic programming. *Quantum Information Processing*, 17(3):67, Feb 2018.
- [3] Kavita Dorai, T. S. Mahesh, Arvind Kumar, and Anil Kumar. Quantum computation using nmr. *Current Science*, 79(10):1447–1458, 2000.
- [4] Michael Goerz et al. Welcome to the krotov package’s documentation. [https://qucontrol.github.io/krotov/v1.0.0/11\\_other\\_methods.html#choosing-an-optimization-method](https://qucontrol.github.io/krotov/v1.0.0/11_other_methods.html#choosing-an-optimization-method), 2019. Online; accessed 04 April 2021.
- [5] Navin Khaneja, Timo Reiss, Cindie Kehlet, Thomas Schulte-Herbrüggen, and Steffen J. Glaser. Optimal control of coupled spin dynamics: design of nmr pulse sequences by gradient ascent algorithms. *Journal of Magnetic Resonance*, 172(2):296 – 305, 2005.
- [6] S. Machnes, U. Sander, S. J. Glaser, P. de Fouquières, A. Gruslys, S. Schirmer, and T. Schulte-Herbrüggen. Comparing, optimizing, and benchmarking quantum-control algorithms in a unifying programming framework. *Physical Review A*, 84(2), Aug 2011.
- [7] A. Mazumder and D.K. Dubey. Nuclear magnetic resonance (nmr) spectroscopy. In *Reference Module in Chemistry, Molecular Sciences and Chemical Engineering*. Elsevier, 2013.
- [8] Ivan S. Oliveira, Tito J. Bonagamba, Roberto S. Sarthour, Jair C.C. Freitas, and Eduardo R. deAzevedo. 2 - basic concepts on nuclear magnetic resonance. In Ivan S. Oliveira, Tito J. Bonagamba, Roberto S. Sarthour, Jair C.C. Freitas, and Eduardo R. deAzevedo, editors, *NMR Quantum Information Processing*, pages 33 – 91. Elsevier Science B.V., Amsterdam, 2007.

- [9] Ivan S. Oliveira, Tito J. Bonagamba, Roberto S. Sarthour, Jair C.C. Freitas, and Eduardo R. deAzevedo. 3 - fundamentals of quantum computation and quantum information. In Ivan S. Oliveira, Tito J. Bonagamba, Roberto S. Sarthour, Jair C.C. Freitas, and Eduardo R. deAzevedo, editors, *NMR Quantum Information Processing*, pages 93 – 136. Elsevier Science B.V., Amsterdam, 2007.
- [10] Ivan S. Oliveira, Tito J. Bonagamba, Roberto S. Sarthour, Jair C.C. Freitas, and Eduardo R. deAzevedo. 4 - introduction to nmr quantum computing. In Ivan S. Oliveira, Tito J. Bonagamba, Roberto S. Sarthour, Jair C.C. Freitas, and Eduardo R. deAzevedo, editors, *NMR Quantum Information Processing*, pages 137 – 181. Elsevier Science B.V., Amsterdam, 2007.
- [11] Benjamin Rowland and Jonathan A. Jones. Implementing quantum logic gates with gradient ascent pulse engineering: principles and practicalities. *Philosophical Transactions of the Royal Society A: Mathematical, Physical and Engineering Sciences*, 370(1976):4636–4650, Oct 2012.
- [12] Ryan, Colm. *Characterization and Control in Large Hilbert spaces*. PhD thesis, 2008.
- [13] Yehuda Sharf, Timothy F. Havel, and David G. Cory. Spatially encoded pseudopure states for nmr quantum-information processing. *Physical Review A*, 62(5), Oct 2000.
- [14] Harpreet Singh, Arvind, and Kavita Dorai. Constructing valid density matrices on an nmr quantum information processor via maximum likelihood estimation. *Physics Letters A*, 380(38):3051–3056, 2016.
- [15] Jens Jakob Sørensen, Jacob Søgaard Nyemann, Felix Motzoi, Jacob Sherson, and Thomas Vosegaard. Optimization of pulses with low bandwidth for improved excitation of multiple-quantum coherences in nmr of quadrupolar nuclei. *The Journal of Chemical Physics*, 152(5):054104, 2020.
- [16] Zdeněk Tošner, Thomas Vosegaard, Cindie Kehlet, Navin Khaneja, Steffen J. Glaser, and Niels Chr. Nielsen. Optimal control in nmr spectroscopy: Numerical implementation in simpson. *Journal of Magnetic Resonance*, 197(2):120–134, 2009.
- [17] Jingfu Zhang, Alexandre M. Souza, Frederico Dias Brandao, and Dieter Suter. Protected quantum computing: Interleaving gate operations with dynamical decoupling sequences. *Phys. Rev. Lett.*, 112:050502, Feb 2014.